Pancreatic beta-cell-specific deletion of insulin-degrading enzyme leads to dysregulated insulin secretion and beta-cell functional immaturity

Cristina M Fernández-Díaz [1], Beatriz Merino [1], José F López-Acosta [1], Pilar Cidad [1], Miguel A de la Fuente [1], Carmen D Lobatón [1], Alfredo Moreno [1], Malcolm A. Leissring[3], Germán Perdomo [4], Irene Cózar-Castellano [1,2*]

[1]Instituto de Biología y Genética Molecular-IBGM (Universidad de Valladolid-CSIC), Valladolid, Spain.

[2]Centro de Investigación Biomédica en Red de Diabetes y Enfermedades Metabólicas Asociadas (CIBERDEM), Madrid, Spain

[3]Institute for Memory Impairments and Neurological Disorders, University of California, Irvine (UCI MIND), Irvine, CA, USA.

[4]Departmento de Ciencias de la Salud, Facultad de Ciencias de la Salud, Universidad de Burgos, Burgos, Spain.

*Corresponding author

Irene Cózar-Castellano, PhD

Instituto de Biología y Genética Molecular (IBGM)/Dpt. Biochemistry and Physiology

School of Medicine, University of Valladolid

Ramón y Cajal, 7, 47005 Valladolid (Spain)

Tel: +34- 983184005

ORCID: 0000-0002-6065-5362

Word number in main text: 5,980

Figure number: 9 Figures + 4 supplemental Figures

Abstract

Inhibition of insulin-degrading enzyme (IDE) has been proposed as a possible therapeutic target for type 2 diabetes treatment. However, many aspects of IDE's role in glucose homeostasis need to be clarified. In light of this, new preclinical models are required to elucidate the specific role of this protease in the main tissues related to insulin handling.

To address this, here we generated a novel line of mice with selective deletion of the Ide gene within pancreatic beta-cells, B-IDE-KO mice, which have been characterized in terms of multiple metabolic endpoints, including blood glucose, plasma C-peptide and ipGTT. In addition, glucose-stimulated insulin secretion was quantified in isolated pancreatic islets, and beta-cell differentiation markers and insulin secretion machinery were characterized by RT-PCR. Additionally, IDE was genetically and pharmacologically inhibited in INS-1E cells, rodent and human islets, and insulin secretion was assessed.

Our results show that, in vivo, life-long deletion of IDE from beta-cells results in increased plasma C-peptide levels. Corroborating these findings, isolated islets from B-IDE-KO mice showed constitutive insulin secretion, a hallmark of beta-cell functional immaturity. Unexpectedly, we found 60% increase in Glut1 (a high affinity/low Km glucose transporter), suggesting increased glucose transport into the beta-cell at low glucose levels, which may be related to constitutive insulin secretion. In parallel, IDE inhibition in INS-1E and islet cells resulted in impaired insulin secretion after glucose challenge.

We conclude that IDE is required for glucose-stimulated insulin secretion. When IDE is inhibited, insulin secretion machinery is perturbed, causing either inhibition of insulin release at high glucose concentrations, or constitutive secretion.

Keywords: Beta-cell immaturity, GK, Glut1, Glut2, Insulin-degrading enzyme, insulin secretion

Introduction

Insulin-degrading enzyme (IDE) is a metalloprotease known to degrade several peptides centrally involved in glucose regulation, including insulin, glucagon, and amylin. IDE has a particularly high affinity for insulin (K_m~0.1 μM) and it is ubiquitously expressed (7, 8, 30). IDE has been historically been regarded as the principal protease involved in the degradation of insulin in vivo (8), but this long-held view has been called into question by recent studies (9, 40).

The relationship between IDE and diabetes mellitus has been stimulated by the fact that the *Ide* gene is located in one of chromosomal regions associated with type 2 diabetes susceptibility (33); and there are some polymorphisms of *Ide* that have been associated with the development of the disease (4, 12, 17, 42). Independent of IDE's role in risk for diabetes, several groups have pursued the development of pharmacological inhibitors of IDE based on the idea that blocking insulin degradation by IDE will increase circulating insulin and thus improve glycemic control in diabetes (6, 9, 24, 26, 30). Results obtained by these studies have been contradictory, perhaps due to pleiotropic effects of IDE inhibition within different organs and target tissues. Thus, it is clear that cell-type specific information is required to properly assess whether IDE inhibition can be a therapeutic target for diabetes mellitus.

We and others have previously reported that beta-cells of type 2 diabetes patients show decreased IDE protein levels, which it is probably related to beta-cell dysfunction (11, 29, 34). Steneberg and colleagues have shown that islets isolated from *Ide* knock-out mice display impaired glucose stimulated insulin secretion (34); whether this effect is attributable to *Ide* deletion in the pancreatic beta-cells specifically needs to be clarified since they used germ-line, pan-cellular knock-out mice for their experiments, which are known to undergo significant age-dependent changes as they develop (1).

In this study we have addressed whether acute pharmacological inhibition of IDE in isolated islets has an effect on pancreatic islet cells´ function; and if IDE is required for beta-cell function. We have used three different tools to investigate these questions: isolated rodent and human islets treated with pharmacological inhibitors of IDE; INS-1E cells knock-down for *Ide*; and a novel mouse model of beta-cell specific ablation of IDE (B-IDE-KO).

Material and Methods

B-IDE-KO mice

Animal experiments were approved by University of Valladolid Research Animal Ethical Committee and JCyL regional authorities (protocol #5003931) in accordance with the European Guidelines for Care and Use of Mammals in Research. The Cre/LoxP system was used for generating our tissue specific knockout mice. *IDE $^{Flox/Flox}$* mice (1, 40) were crossed to *Ins2-Cre* mice provided by Dr. Herrera (Ins2.Cre^{Herr}) (15). The breeding strategy is explained more fully in Fig 4A. *IDE$^{Flox/Flox}$;Ins-Cre* mice are the beta-cell specific IDE KO mice (B-IDE-KO) and *IDE$^{Flox/Flox}$ and IDE$^{Flox/+}$* have been used as control mice (WT). *IDE$^{Flox/+}$;Ins-Cre* (HT) have not been characterized in this manuscript.

To genotype the colony of mice, PCR was performed with tail DNA isolated using QuickExtract™ DNA Extraction Solution (Epicentre, USA) according to the manufacturer's instructions. The primers used for PCR were as follows: GAPDH_R: *5'-GATG GCAT GGA CTG TGG TCA T-3'*; GAPDH_F: *5'-CGT GGA GTC TAC TGG TGT CTT-3'*; FLOX-IDE_F: *5'-AAC TGC CAC CTG TCC AAT CC-3'*; FLOX-IDE_R: *5'-CTC AGG GAT ACA ATG CGT GC-3'*; INS-CRE_F: *5'-TAA GGC TAA GTA GAG GTG T-3'*; INS-CRE_R: *5'-TCC ATG GTG ATA CAA GGG AC-3'*.

Male and female animals were metabolically characterized at 2 and 6 months. Mice were fed standard rodent chow diet and water *ad libitum* in ventilation-controlled cages in a 12-hour light/dark cycle.

High-fat diet experiments

In order to metabolically stress B-IDE-KO and controls, 6-month-old male mice were fed a high-fat diet (60% kcal fat, Research Diets, USA) for four weeks. Afterwards ipGTT and C-peptide levels in circulation were measured.

Plasma biochemistry

Blood glucose levels at 16h or 6h fasting and non-fasting conditions were measured directly from tails using the Breeze2 Glucometer (Bayer, Germany). Plasma samples were obtained from tail blood samples of mice under fasting (6h) or non-fasting conditions, blood was extracted using blood collection tubes treated with EDTA (Sarstedt AG & Co., Germany). Plasma C-peptide levels were measured using Mouse Ultrasensitive C-peptide ELISA (#80-CPTMS-E01, ALPCO, Salem, NH). Amylin levels were measured using mouse amylin enzyme immunoassay (EIA) kit (#EK-017-11, Phoenix Pharmaceuticals, USA).

Intraperitoneal glucose tolerance test

To evaluate alterations in glucose homeostasis in our mice, we performed intraperitoneal glucose tolerance tests (ipGTT). Briefly, mice were fasted for 6 h and then injected intraperitoneally with glucose at 2 g/kg body weight. Blood glucose levels were quantified immediately before and 15, 30, 60 and 120 min after glucose challenge.

In a different set of experiments, but using the same technique, blood samples were obtained 0, 5, 15 and 30-minutes after glucose challenge using blood collection tubes. Plasma was obtained by centrifuging the blood at 3,300 X g for 10 min. C-peptide levels were determined by ELISA as described above.

RNA isolation and RT-PCR

Total RNA from islets and tissues samples was extracted using TRIZol® Reagent (Thermo Fisher Scientific, USA), according to the manufacturer's instructions. Quantification of mRNA levels was determined from UV absorbance using a NanoDrop™ N-D1000 spectrophotometer. These samples were treated with RapidOut DNA Removal Kit (Thermo Fisher Scientific, USA). First strand complementary DNA (cDNA) was synthesized with iScript™ cDNA synthesis kit (Bio-Rad, USA) as described in the manufacturer's instructions.

Quantitative PCR was carried out on equal amounts of cDNA in duplicate for each sample using Maxima Probe qPCR Master Mix (Thermo Fisher Scientific, USA) with corresponding TaqMan® Gene Expression Assays (Applied Biosystems, USA) in a thermal cycler Rotor-Gene 3000 (Corbett Research). The following TaqMan assays were used: *Ide*: Mm00473077_m1; *Ins1*: Mm01259683_g1; *Ins2*: Mm00731595_gH; *Nkx2-2*: Mm00839794_m1; *Nkx6-1*: Mm00454961_m1; *Pax6*: Mm00443081_m1; *Pdx1*: Mm00435565_m1; *Neurod1*: Mm_01280117_m1; *Mafb*: Mm00627481_s1; *Ucn3*: Mm00453206_s1; *Syt4*: Mm01157571_m1; *Slc2a2*: Mm00446229_m1; *Slc2a1:* Mm00441480_m1; *Slc2a3:* Mm00441483_m1; *Gck*: Mm00439129_m1; *Kcnj11*: Mm00440050_s1; *Abcc8*: Mm00803450_m1; C*acna1a*: Mm00432190_m1; *G6pc*: Mm00839363_m1; *Pck1*: Mm01247058_m1. The following SYBR Green assay was used: *Mafa*: (F: 5´-GAGGAGGTCATCCGACTGAAA-3´; R: 5´-GCACTTCTCGCTCTCCAGAAT-3´) *Pcsk1:* (F: 5'-CTGGCCAATGGGTCGTACTC-3'; R: 5'-TGGAGGCAAACCCAAATCTTAC- 3').

Data were normalized with the housekeeping gene *RPL18*: (F: 5'-AAGACTGCCGTGGTTGTGG-3´; R: 5'-AGCCTTGAGGATGCGACTC-3', Probe: 5'-FAM-TTCCCAAGCTGAAGGTGTGTGCA-BHQ1-3') and relative expression was quantified using the comparative $2^{-\Delta\Delta CT}$ method.

Quantification of islet histomorphometry

Six-month-old mice were euthanized, their pancreata were dissected and fixed in 10% neutral buffer formalin overnight at 4 °C, then embedded into paraffin blocks. Five-µm sections were obtained from 4 distinct areas of each pancreas spaced at least 100 microns. To analyze pancreatic morphology pancreas sections were stained with anti-insulin antibody 1:100 dilution (#180067, Invitrogen, USA) for beta-cell area and anti-glucagon antibody 1:500 dilution (#10988, Abcam, UK) for alpha-cell area, and they were counterstained with hematoxylin, as previously reported (20).

Images of the sections were acquired using a NIKON Eclipse 90i microscope associated with CCD NIKON camera (DSRi1), using 20X objective with transmitted light. Beta-cell area, alpha-cell area and islet number were calculated using ImageJ software (NIH, USA) as previously reported (20, 40).

Cell culture

INS-1E were a gift of Dr. Pierre Maechler (University of Geneva, Switzerland). Cells were grown at 37 °C and 5% CO_2 in a humidified atmosphere to 80% confluence. INS-1E culture medium was RPMI-1640 with 2 mM L-glutamine supplemented with 11 mM D-glucose, 10% fetal bovine serum, 100 U/ml penicillin, 100 µg/ml streptomycin, 10 mM HEPES, 1 mM sodium pyruvate, and 50 µM β-mercaptoethanol. Mycoplasma contamination was checked monthly.

Small interfering RNA-mediated gene suppression

ON-TARGET plus SMART pool siRNA targeting Rat IDE (Dharmacon, USA) was transfected into INS-1E cells in the presence of Lipofectamine 2000 Transfection Reagent (Invitrogen, USA) for 4h. Cells were cultured for 72h in INS-1E cell medium before experimentation. ON-TARGET plus Non-targeting pool was used as control siRNA.

Generation of INS1-E shRNA-IDE

INS-1E cells were transduced using short hairpin RNA (shRNA) lentiviral vector pGreenPuro™ shRNA Cloning and Expression Lentivector (System Biosciences, USA). Oligonucleotide design and shRNA synthesis was performed according to manufacturer´s criteria. The sequences contain both sense and anti-sense strand were located in exon 25 of the rat IDE gene (F: 5´-CCCTTGTGAAGCCACACATTA-3´; R: 5´-CCCTTGTGAAGCCACACATTA-3´). All constructs were sequence-verified. Analysis of silencing efficiency was performed by western blotting.

In-vitro glucose-stimulated insulin secretion

INS-1E cells were seed on cell culture 6-well plates at a density of 600,000 cells per well. After treatment, cells were washed in HEPES balanced salt solution (HBSS) (114mmol/l NaCl, 4.7 mM KCl, 1.2 mM KH_2P O4, 1.16 mM $MgSO_4$, 20 mM HEPES, 2.5 mM $CaCl_2$, 25.5 mM $NaHCO_3$, and 0.2% bovine serum albumin [essentially fatty acid-free], pH 7.2). Insulin secretion was stimulated by using static incubation for a 1-hour period in 3 ml of the same buffer, followed by incubation in HBSS containing 22 mM glucose for 90 min. Insulin secretagogues were used at the following concentrations: 10 mM Arginine (Arg) and 100 µM IBMX. Secretion samples were used to measure insulin by Rat Insulin ELISA (#10-1250-01) and C-peptide by Rat C-peptide ELISA (#10-1172-01). To quantify intracellular insulin content, cells were treated for 1 hour with acid ethanol followed by Rat Insulin ELISA.

Rat and human islets were plated on cell culture inserts onto 24-well plates at a density of 20 IEq groups in HBSS. Islets were washed twice in 1 ml HBSS with 2.2 mM glucose followed by preincubation in 2 ml of the same buffer for 10 min. Insulin secretion was stimulated by using static incubation for 30 min in 1 ml of the same buffer, followed by incubation in HBSS containing 22 mmol/l glucose for 30 min. Secretion samples of rat islets were used to measure insulin by Rat Insulin ELISA. Secretion samples of human islets were measured by Insulin ELISA (#10-1113-01). Secreted insulin was represented dividing by islet number in GSIS.

B-IDE-KO islets were plated on cell culture inserts in 24-well plates at a density of 5 equivalent islets per well. Islets were washed twice in 500 µl Krebs-Ringer buffer (140 mM NaCl, 4.5 mM KCl, 1 mM MgCl2, 25 mM HEPES, 2.5 mM CaCl2, 0.1% BSA) with 3 mM glucose. Insulin secretion was stimulated by using static incubation for 1 h in 500 µl of the same buffer, followed by incubation in KRB containing 16 mmol/l glucose for 1 h. Secretion samples were used to measure insulin by Mouse Insulin ELISA (#10-1247-01) and proinsulin by Rat/Mouse Proinsulin ELISA (#10-1232-01). To analyze the intracellular insulin content, islets were exposed for 1 h to acid ethanol followed by quantification using Mouse Insulin ELISA. Secreted insulin was represented dividing by islet number in GSIS.

All insulin, proinsulin and C-peptide ELISA kits reported in here were obtained from Mercodia AB, Sweden.

Islets isolation and culture

B-IDE-KO islets were isolated by pancreatic duct perfusion with Collagenase P (1.7 mg/mL) (Roche Diagnostics, USA) and purified as previously reported (5) from 6-month-old male mice. To quantify intracellular insulin content, islets were exposed for 1 hour to acid ethanol followed

by Mouse Insulin ELISA, and normalized to the DNA content of the sample, measured using a NanoDrop™ N-D1000 spectrophotometer.

Rat islets were isolated and purified from 2-month-old male Wistar rats provided by Animal Production and Experimentation Service (University of Valladolid) by a standard procedure and they were grown at 37°C and 5% CO_2 in a humidified atmosphere. Culture medium was RPMI-1640 (GIBCO, EEUU) supplemented with 5.5 mM D-glucose, 10% fetal bovine serum, 100 U/ml penicillin, and 100 µg/ml streptomycin.

Human islets were obtained from Dr. Olle Körsgren lab at the University of Uppsala (Sweden) through Juvenile Diabetes Research Foundation award 31-2008-416 (ECIT Islet for Basic Research program). Islets were grown at 37 °C and 5% CO_2 in a humidified atmosphere. Culture medium was RPMI-1640 (GIBCO, EEUU) supplemented with 5.5 mM D-glucose, 10% fetal bovine serum, 100 U/ml penicillin, and 100 µg/ml streptomycin.

Western blotting

Islets from B-IDE-KO mice and INS-1E cells were homogenized in lysis buffer (125 mM Tris, pH 6.8, 2% SDS, 1 mM DTT supplemented with protease and phosphatase inhibitors) and briefly sonicated. Proteins were quantified using the Micro BCA Kit (Thermo Scientific, USA), separated by SDS-PAGE (7.5%), and then transferred to PDVF Immobilon-P membranes (Millipore, USA). Blots were incubated with the following antibodies: anti-Actin 1:40,000 dilution (#612656, BD Biosciences, USA), anti-IDE 1:15,000 dilution (#9210, Millipore, USA), anti-GLUT1 1:10,000 dilution (#07-1401, Millipore, USA), anti-GLUT2 1:10,000 dilution (#07-1402 Millipore, USA), anti-GCK 1:5,000 dilution (#ab37796, Abcam, UK), anti-GAPDH 1:10,000 (#mab374, Chemicon international, USA). All antibodies were previously validated by the manufacturer and previous publications (11, 40).

ImageJ software (NIH, USA) was used for processing and analysis of data. Results were normalized to control values on each membrane.

Electron microscopy

After performing GSIS on INS1-E cells, pellets of cell preparations were fixed in 2% formaldehyde and 2% glutaraldehyde in phosphate buffered saline (PBS) for 30 min at 4 °C. Samples were then embedded in 2% agar, post-fixed with 1% osmium tetroxide in water, dehydrated through a graded series of ethanol and embedded in Epoxy EMbed-812 resin (EMS, Electron Microscopy Sciences). Ultrathin sections were obtained with a Leica EM UC7 ultramicrotome, contrasted with uranyl acetate and lead citrate, and analyzed using a Tecnai Spirit Twin 120 kv electron

microscope with a CCD Gatan Orius SC200D camera with DigitalMicrograph™ software. Electron microscopy pictures were taken in the Microscopy Service at the University of Salamanca, Spain.

Inhibition of proteolytic activity

Rat and human islets were treated with the IDE specific inhibitor NTE-2 (kindly provided by Dr. Timothy B. Durham at Eli Lilly and Company, USA) (9) at 0.1 µM. NTE-2 was dissolved in DMSO. Islets were treated with this compounds or its respective vehicle for 1h at 37 °C in complete medium before glucose-stimulated insulin secretion.

Immunostaining

B-IDE-KO pancreata were dissected and immersed in 10% neutral buffer formalin overnight and embedded into paraffin blocks. Five-µM serial sections of pancreas were obtained and stained with the following antibodies: Mouse anti-insulin 1:1,000 dilution (#SAB4200691, Sigma-Aldrich, USA), rabbit anti-IDE 1:2,000 dilution (#9210, Millipore, USA), rabbit anti-Glut-1 1:500 dilution (#07-1401, Millipore, USA) and rabbit anti-glut-2 1:500 dilution (#07-1402 Millipore, USA). Fluorescent secondary antibodies were used for detection. All antibodies were previously validated by the manufacturer and previous publications (3, 11, 19, 39). Sections were counterstained with nuclear DAPI staining. Fluorescence images of the sections were acquired using a NIKON Eclipse 90i microscope associated with CCD NIKON camera (DSRi1), using a 40X objective. All the pictures were obtained using the same exposure conditions.

Immunofluorescence intensity of Glut1 was quantified by ImageJ software (NIH, USA) using the following method to each insulin/Glut1 stained pancreas slide: Separated photos of insulin and Glut1 were taken. A mask of the insulin stained area was made using the “Create Mask” tool on the insulin photo. The mask of insulin area was transferred onto the Glut1 photo, and then, the intensity of Glut1 staining within this selected “mask” area was quantified using the tool “Integrated Density”. The final intensity number was calculated dividing integrated density/mask area.

Statistics

Data were analyzed using the Graph Pad Prism v. 4.0 (GraphPad Software, Inc., La Jolla, CA, USA). Data were presented as mean ± SEM. Distribution of variables was analyzed using the Kolmogorov-Smirnov test. Statistical differences between two groups were analysed using the Student's t-test and between more than two groups using an ANOVA test followed by Tukey’s multiple comparison test. A significance level of <0.05 was used to judge statistical significance.

Results

IDE inhibition of adult beta-cells impairs insulin secretion

To clarify whether the presence of IDE plays a key role in beta-cell function, we tested insulin secretion in the pancreatic beta cell line INS-1E transfected with siRNA-IDE or control si-RNA. As judged by western blot analysis, we obtained ~40% reduction of IDE levels (Fig 1A-B). Upon challenge with low and high glucose, INS-1E cells with reduced IDE levels exhibited a ~50% decrease in secreted insulin relative to controls (Fig 1C).

To assess whether the observed result was due to a defect on the machinery of secretion or, instead, an effect on insulin stability or production, we quantified C-peptide levels in same cell culture supernatants. C-peptide levels in the IDE-deficient INS-1E cells were significantly decreased by 50% relative to controls, in excellent agreement with the results for insulin secretion (Fig 1D). No alterations in intracellular insulin content were detected (Fig 1E). Together, these results indicate that insulin secretion is impaired when IDE levels are reduced in INS-1E cells.

To confirm our results using a different model that ensures uniformity of IDE silencing over a more prolonged period of time, we generated an INS-1E clone using lentiviruses containing shRNA-IDE (INS1-shRNA-IDE), which expressed IDE protein levels reduced by ~30% relative to a control clone (INS1-shRNA-C) generated in parallel (Fig 2A-B). INS1-shRNA-IDE cells showed total abolishment of insulin secretion upon either high or low glucose challenge (Fig 2C). Interestingly, insulin content was increased by 100% in INS1-shRNA-IDE cells (Fig 2D). To elucidate the mechanistic basis underlying the observed impairment in insulin secretion, we studied INS1-shRNA-IDE cell ultrastructure by electronic microscopy, which revealed an approximate doubling of the density of insulin granules in INS1-shRNA-IDE cells after glucose overload versus INS1-shRNA-C cells, pointing to a defect in insulin vesicle mobility (Fig 2E-F). Supporting this conclusion, in GSIS experiments, insulin release in the presence of two insulin secretagogues, Arg and IBMX, was impaired in INS1-shRNA-IDE cells relative to control cells (Suppl Fig 1).

To explore a more physiological model, we obtained isolated islets from rat and human pancreata and pharmacologically inhibited IDE activity using the IDE specific inhibitor NTE-2. Both assays showed a significant impairment in insulin secretion (Fig 3 A-B), corroborating the results obtained from INS-1E cells in Figures 1 and 2.

Taken together, these results indicate that acute reduction or inhibition of IDE in INS-1 cells or islet cells in vitro leads to impaired glucose-stimulated insulin secretion (GSIS). However, these

experiments do not address the effect of chronic deficiency of IDE, specifically in beta-cells, nor do they reveal any insight into the role of IDE in the beta-cell in vivo. For that purpose, we generated beta-cell specific IDE knock-out mice.

B-IDE-KO mice show normal glucose homeostasis despite increased C-peptide in circulation

Pancreatic beta-cell specific IDE knock-out mice (B-IDE-KO) were generated by breeding mice homozygous for a floxed *Ide* allele (40) with transgenic mice expressing *Cre* recombinase under the insulin promoter (Ins2.Cre^{Herr}), thus targeting expression to pancreatic beta-cells (15) (Fig 4A). We studied the phenotype of male and female *Ide$^{flox/flox}$; +/+* or *Ide$^{flox/+}$; +/+* (henceforth referred to as WT) and *Ide$^{flox/flox}$; Ins-Cre/+* (B-IDE-KO) mice at 2 and 6 months of age.

To confirm that *Ide* genetic ablation was specific to pancreatic beta-cells, we performed IDE quantitative PCR of B-IDE-KO and WT pancreatic islets, skeletal muscle, kidney, liver and hypothalamus. We found a ~70% reduction of IDE expression in islets, and no changes in the other tissues (Fig 4B).

To verify loss of IDE expression in pancreatic beta-cells, pancreatic islets were obtained from WT, B-IDE-HET (*Ide$^{flox/+}$; Ins-Cre/+*), B-IDE-KO and from T-IDE-KO (germ-line, total-IDE-KO) mice (1) and quantified by western blotting. As expected, IDE was present in islet cells of WT mice, partly reduced in islets of B-IDE-HT mice and mostly absent in B-IDE-KO islets. There is a faint IDE band at 110 kDa in B-IDE-KO, which is not present in the T-IDE-KO extract, which is due to ~20% non-beta-cells present in pancreatic islets (Fig 4C). We also performed IDE/insulin double staining to confirm that IDE loss of expression was specifically happening in beta-cells and not in other islet cell types. As shown in Figure 4D, WT islets show overlapped staining of IDE and insulin, meanwhile B-IDE-KO mice only show IDE staining in non-beta-cells. Together, these results confirm that IDE ablation in B-IDE-KO pancreatic beta-cells was both effective and specific.

We next performed a metabolic characterization of male mice at 2 months of age. First, we measured basal blood glucose levels under fasting (16- and 6-hour) and non-fasting conditions. Relative to WT controls, B-IDE-KO mice didn´t show changes in glucose levels (Fig 5A-C). Glucose homeostasis as measured by ipGTT was normal as showed by the AUC (Fig 5D-E). No changes in body weight were detected (Fig 5F). To understand if IDE has a role in GSIS *in vivo*, plasma C-peptide levels were monitored before and 5, 15 and 30 min after glucose challenge. The resulting AUC indicated that C-peptide in circulation was similar in WT and B-IDE-KO mice (Fig

342 5G-H). Interestingly, *ex vivo* GSIS results obtained in islets isolated from B-IDE-KO and WT mice
343 (Fig 6I) showed that secreted insulin levels were chronically higher in B-IDE-KO islets relative to
344 controls, but no further increase was observed upon high glucose challenge (Fig 6I).
345 Furthermore, GSIS is impaired in B-IDE-KO as shown by the fold-increase in insulin secretion
346 ~3.5-fold *versus* ~1-fold for WT *versus* B-IDE-KO islets, respectively (Fig 6J).

347 Then, we aged mice to 6 months of age and performed a similar metabolic characterization; we
348 measured basal blood glucose levels under fasting (16- and 6-hour) and non-fasting conditions.
349 No changes were observed under fasting or non-fasting conditions (Fig 6A-C). C-peptide levels
350 were increased in B-IDE-KO versus WT mice under both fasted and non-fasted conditions (~60%
351 more) (Fig 6D-E). Glucose homeostasis as measured by ipGTT was normal as showed by the AUC,
352 albeit glucose levels were significantly increased in B-IDE-KO mice 15 minutes after glucose
353 challenge (Fig 6F-G). This metabolic phenotype pointing to increased insulin resistance is not
354 associated to body weight changes (Fig 6H) but it is related to increased hepatic gluconeogenesis
355 as it is suggesting increased expression of phosphoenolpyruvate carboxykinase (*Pck1*) and
356 glucose-6-phosphatase (*G6pc*) enzymes (Fig 6I).

357 Female mice data for ipGTT and plasma C-peptide at 2 and 6 months of age showed similar
358 results to those reported for male mice (Suppl Fig 2).

359 To further potentiate the metabolic phenotype, 6-month-old male B-IDE-KO and WT mice were
360 fed a high-fat diet for 4 weeks. After metabolic characterization, no differences were observed
361 in ipGTT despite the presence of elevated C-peptide levels in B-IDE-KO mice (Suppl Fig 3).

362 Taken together, these results suggest that life-long genetic deletion of IDE in beta-cells results
363 in increased insulin secretion together with a degree of insulin resistance as evidenced by
364 elevated glucose 15 minutes after glucose challenge, in parallel to elevated levels of liver´s
365 gluconeogenic enzymes.

366 C-peptide levels were measured before, 5, 15 and 30 min after glucose challenge. C-peptide
367 levels were increased in each time point, and the resulting AUC was found to be significantly
368 increased as well (Fig 7A-B). This rise in C-peptide levels was not due to increased beta-cell area
369 (Fig 7C-D), alpha-cell area (7 E-F) or number of pancreatic islets (7G); but instead was due to
370 constitutive insulin secretion, as reflected by GSIS results obtained in islets isolated from B-IDE-
371 KO and WT mice (Fig 7H). Secreted insulin was constitutively elevated in B-IDE-KO islets relative
372 to controls, but no further increase was observed upon high glucose challenge (Fig 7H), same as
373 observed in 2 months old mice. Furthermore, GSIS is impaired in B-IDE-KO as shown by the fold-
374 increase in insulin secretion ~2.5-fold versus ~1-fold for WT versus B-IDE-KO islets, respectively

(Fig 7I). No changes were detected in islet insulin content when B-IDE-KO and WT islet extracts were compared (Fig 7J).

Constitutive insulin secretion is a signal of beta-cell immaturity (2, 18, 31) that is often accompanied by increased proinsulin secretion due to a defect in proinsulin processing (13, 16, 43). Accordingly, we measured proinsulin secretion after challenge with low and high glucose. Secreted proinsulin levels show the same profile as insulin secretion, constitutive proinsulin secretion in B-IDE-KO islets (Fig 7K). 1-3% non-processed proinsulin has been previously reported to be secreted with mature insulin in normal islets (13), as it is shown in our WT islets. Here we are showing higher levels of secreted proinsulin in B-IDE-KO islets under low glucose concentrations, in line with the increased insulin levels being secreted under this condition.

B-IDE-KO islets undergo molecular changes that reflect beta-cell functional immaturity

B-IDE-KO islets display a phenotype of constitutive insulin secretion and insulin granules harboring proinsulin molecules, both hallmarks of beta-cell functional immaturity. To attempt to elucidate the molecular mechanisms underlying immature beta-cell phenotype, we performed RT-PCR to quantify mRNA levels of several transcription factors and proteins known to be required for beta-cell maturity (*Ins1, Ins2, Nkx2.2, Nkx6.1, Pax6, Pdx1, Neuro D1, Mafb, Mafa, Ucn3, Syt4*) (Fig 8A). We also quantified the expression of a number of proteins subserving insulin processing (*Pcsk1*) (Fig 8C) and insulin secretion (*Slc2a2, Slc2a1, Salc2a3, Gck, Kcnj11, Abcc8, Cacna1a*) (Fig 8B).

Among the genes reflective of beta-cell maturity B-IDE-KO islets exhibited a 60% decrease in *Ins2* and 40% decrease in *Ucn3* (Fig 8A). Enzymes involved in insulin processing Pcsk1/3, showed a ~70% decrease in B-IDE-KO islets (Fig 8B); this result explains increased proinsulin levels (Fig 7H). Interestingly, we also found that most of the genes involved in insulin secretion (genes codifying for Glut1, GK, Sur1 and calcium channel) are upregulated, which is reflective of activation of cell metabolism and constitutive insulin secretion. Especially relevant is the increase in *Scl2a1* (Glut1 gene) levels observed in B-IDE-KO islets, which is the main glucose transporter in alpha-cells, but not in beta-cells. At the same time *Scl2a2 (*Glut2 gene), which is the main glucose transporter in mouse beta-cells, is unchanged. The K_m value is an indicator of the affinity of the glucose transporter for glucose molecules; Glut2 K_m is 15-20 mM, meanwhile Glut1 K_m is 1-3 mM (23); therefore, Glut1 has a high affinity for glucose and uptake from extracellular medium is constant.

To further elucidate the mechanisms underlying constitutive insulin secretion in B-IDE-KO islets, we immunostained pancreata of WT and B-IDE-KO mice with Glut2 and Glut1 antibodies (Fig 9 A-B). B-IDE-KO beta-cells showed less Glut2 in the plasma membrane (Fig 9A), meanwhile Glut1 expression was increased in B-IDE-KO pancreatic beta-cells (Fig 9B). Quantification of Glut1 staining in the insulin-positive area showed a 50% increase in Glut1 expression in B-IDE-KO versus WT beta-cells (Fig 9C). These results were confirmed by western-blot of protein extracts obtained from isolated islets (Fig 9D). The following proteins were detected and quantified: IDE, GK, Glut1 and Glut2. These experiments demonstrated that Glut 1 levels were ~60% upregulated, and there were not changes in GK or Glut2 total levels. These results suggest that abnormal glucose transport under low glucose concentrations may occur in B-IDE-KO but not WT pancreata due to elevated Glut1 levels, which in turn would result in continuous glucose utilization. Interestingly, although Glut2 total protein levels are not changed in B-IDE-KO islets by western-blot, staining shows reduced localization at the plasma membrane compared with WT beta-cells (Fig 9A). This phenotype of Glut2 has been shown in other beta-cell immaturity models (22, 31).

The abnormal pattern of glucose transporters in B-IDE-KO beta-cells due to IDE loss of expression may be associated to constitutive and impaired insulin secretion in B-IDE-KO mice.

Discussion

IDE's precise role in glucose homeostasis remains unresolved, as evidenced by contradictory results observed in germ-line Total-IDE-KO mice (1, 10, 34) and also following administration of IDE inhibitors to diabetic mouse models (6, 9, 24, 26). Since IDE is a ubiquitous protein, total knock-out models, or pharmacological inhibitors, can only reveal overall metabolic results, potentially obscuring complex interactions and thereby limiting the understanding of IDE's tissue-specific roles in glucose homeostasis. The generation of cell-specific IDE KO models can facilitate the elucidation of the precise role of IDE in different tissues involved in glucose and insulin homeostasis.

Since its discovery in 1949 (27), the primary function of IDE—indeed that implied by the name "insulin-degrading enzyme"—has been widely supposed to be limited to that of proteolytic degradation of insulin. Initial studies in germ-line Total-IDE-KO models (1, 10) reported that these animals exhibit hyperinsulinemia, seemingly confirming this view. However, subsequent studies utilizing tissue-specific genetic ablation or analyzing tissue-specific functions of IDE have not supported this simplistic model. For instance, Villa-Pérez and colleagues found that,

contrary to expectation, insulin clearance was not impaired by selective deletion of IDE from liver (L-IDE-KO mouse), the primary organ involved in insulin clearance (40). Similarly, Steneberg and colleagues uncovered evidence that insulin secretion from both intact Total-IDE-KO animals and isolated islets is in fact impaired, and traced the cause to a non-proteolytic mechanism associated with insulin secretion that involved the irreversible binding of alpha-synuclein to IDE (34).

In the present study, we aimed to further elucidate the function of IDE by investigating the consequences of genetic and/or pharmacological reduction of IDE selectively in beta cells, using multiple, complementary approaches. Consistent with previous findings suggesting a role for IDE in facilitating insulin secretion (34), decreasing IDE levels in INS-1E cells by shRNA or siRNA resulted in significant decreases in GSIS. Similar results were obtained for human and rat islets treated with pharmacological inhibitors of IDE. The latter results are the first to directly examine the effects of IDE inhibitors on insulin secretion, and they raise the interesting possibility that, whatever the precise role of IDE in beta-cells, its function may involve its proteolytic activity. At the same time, these results would seem to argue against the viability of using IDE inhibitors as a potential treatment for diabetes.

A consistent finding among all papers examining germ-line Total-IDE-KO mice is the development of very marked glucose intolerance by 6 months of age (1, 10, 34). We report here that deletion of IDE in beta-cells does not fully recapitulate the previously observed phenotype. This finding clearly demonstrates that the effects of IDE deletion on glucose homeostasis are not explained by its role in beta-cells on insulin secretion exclusively. Indeed, this conclusion is reinforced by the recent report that liver-specific ablation also results in pronounced effects on glucose tolerance (40). Thus, our study reinforces the idea that IDE has multiple roles within many diverse aspects of glucose regulation, which deserve to be explored further.

Another significant finding is the observation of constitutive insulin secretion in the absence of high glucose in B-IDE-KO mice. After investigating potential mechanisms, we uncovered the novel finding that beta-cells from B-IDE-KO mice harbor decreased levels of the Glut2 glucose transporter in the plasma membrane and increased levels of Glut1. These observations suggest a plausible explanation for the hyperinsulinemia reported in other studies of germ-line Total-IDE-KO mice, which had previously been hypothesized as being due to decreased catabolism of insulin by IDE (1, 10).

We propose two different models of IDE loss of function: an in vitro and acute type of partial loss of function (as exemplified by INS-1E cells and isolated islets), and an in vivo, chronic,

complete loss of function (as exemplified by the B-IDE-KO mouse line). When beta-cells are acutely deprived of IDE expression or activity, GSIS is impaired. These results are in good agreement with those of Steneberg et al. (34), who reported impaired insulin secretion in islets of Total-IDE-KO mice due to a defect of beta-cell cytoskeleton. Here we show that INS1-shRNA-IDE beta-cells also exhibit increases in the amount of insulin granules and augmented insulin content after GSIS, pointing to a defect in the movement of insulin granules consistent with what was described previously (34). More importantly, we are showing for the first time that IDE pharmacological inhibition in human islets cells leads to impaired insulin secretion. These results are in agreement with what we and others have recently published (11, 29, 34), IDE loss of expression occurs in dysfunctional type 2 diabetes human beta-cells. Taken together, our results with human islets support the idea that IDE plays a key role in human beta-cell function.

In contrast to these *in vitro* results, we show here that beta-cell chronic and total loss of IDE expression starting at embryonic life (as in the B-IDE-KO mouse line) generates constitutive insulin secretion. B-IDE-KO islets secrete high quantities of insulin at low glucose and have a stunted secretory response. This result is likely attributable to the dysfunctional phenotype observed in IDE-null beta-cells. Glut 1 is a high-affinity/low- Km transporter that transports glucose at concentrations as low as 1 mM (35). Thus, it is possible that Glut1 would be introducing glucose into the beta-cell at low glucose concentrations, although glucose uptake itself wouldn´t be enough to induce insulin secretion; it is well known that the step limiting in beta-cell glucose metabolism is GK (the glucose sensor) and glucose phosphorylation. We are describing here a novel model where beta-cell glucose transport is possible at low glucose concentrations due to increased Glut1 levels, that it is making possible the entrance of glucose at 2mM extracellular glucose, increasing intracellular glucose levels and activating GK to produce glucose-6-P, glycolysis and increased ATP/ADP ratio that ends producing insulin exocytosis.

Interestingly, although insulin secretion is stimulated at low glucose, there is impaired GSIS when glucose levels increase. This is an unexpected result, since the entire insulin secretion machinery looks hyperactive, as shown by increased expression of glucokinase, potassium channel and calcium channel in B-IDE-KO islets, but it might be explained by decreased levels of Glut2 in the plasma membrane. It is known that Glut2 normal levels are required for a physiological response to high glucose concentrations (38).

Constitutive insulin secretion has been reported as a hallmark of dysfunctional and immature beta-cells. Embryonic and neonatal beta-cells secrete insulin constitutively (2, 14, 18, 31). It is already described that embryonic cells have more Glut1 than any other glucose transporter.

Most fetal cells exhibit rapid growth and differentiation requiring high supply of energy, glucose being one of the most important nutrients required to obtain ATP (25). It will be critical to more deeply explore the mechanisms underlying increased Glut1 levels in the beta-cell plasma membrane in the absence of IDE. Other markers that support beta-cell immaturity in B-IDE-KO islets are decreased mRNA levels of *Ins2* and *Ucn3* (2), increased proinsulin secretion at basal glucose levels, decreased protein convertase 1 (Pcsk1/3) (31) and abnormal pattern of Glut2 in the plasma membrane (18, 22, 31, 36).

Treatment of lean and obese mice with IDE specific inhibitor 6bk shows that IDE regulates the abundance and signaling of glucagon and amylin, in addition to that of insulin (26). In our hands, pancreatic beta-cell specific IDE genetic abolishment is not affecting to other beta-cell´s products that can be degraded by IDE, as amylin (Suppl Fig 4). In Maianti´s manuscript glucagon is upregulated after 135 min of IDE inhibition (26). Alpha-cell specific IDE loss of function experiments are required to elucidate the impact of IDE on glucagon homeostasis.

Despite considerable efforts spanning decades, the etiology of insulin resistance remains to be deciphered. Classically, it has been proposed that intracellular accumulation of toxic lipids, derived from adipose tissue lipolysis, triggers systemic insulin resistance, which in turn increases compensatory beta-cell insulin secretion, leading to hyperinsulinemia. However, it has also been proposed that elevated basal levels of insulin play a causative role of in the pathogenesis of insulin resistance in obesity and type 2 diabetes. Mechanistically, this could be mediated by desensitization and lysosomal degradation of the insulin receptor by chronically elevated levels of circulating insulin, leading to a reduced tissue response to insulin (21, 28, 32, 37).

We show here that selective deletion of IDE in beta cells results in increased basal circulating C-peptide levels, in parallel with hepatic insulin resistance. Mechanistically, insulin resistance was associated with dysregulated hepatic gluconeogenic gene expression of PEPCK (*Pck1*) and G6Pase (*G6pc*). The expression of both genes is inhibited by insulin and requires intact intracellular insulin signaling. PEPCK regulates the rate-limiting step of gluconeogenesis (i.e. the conversion of oxaloacetate into phosphoenolpyruvate), whereas G6Pase catalyzes the final step of gluconeogenesis by converting glucose-6-phosphate to glucose. These results in our B-IDE-KO mouse model beg an important question: How can the interplay between elevated levels of C-peptide and hepatic insulin resistance be explained? Here, we propose the following model: Beta-cell depletion of IDE leads to increased C-peptide/insulin secretion *via* portal vein and chronic exposure of hepatocytes to insulin. In response, chronically elevated insulin causes desensitization and lysosomal degradation of the insulin receptor leading to decreased

intracellular insulin signaling and poor regulation of hepatic gluconeogenic gene expression. In this model, we cannot exclude that other metabolic pathways regulated by insulin may remain intact as a compensatory mechanism to maintain glucose homeostasis (e.g. enhanced hepatic glycogenesis and/or insulin clearance). Further work is warranted to clarify molecular mechanisms of hepatic insulin resistance in the B-IDE-KO mouse model.

Because our B-IDE-KO mice have been generated using Ins2.Cre^{Herr} mice, and it has been reported that this line can generate some low degree of recombination in brain (41), we cannot disregard the impact of that possible recombination in our metabolic phenotype. That said, increased insulin secretion resulting from IDE deletion *in vivo* has also been demonstrated *ex vivo* in isolated islets, where brain-dependent effects are absent. Future studies using a more cell-type specific Cre-LoxP system would help to clarify this point.

Our data highlight the following conclusion: IDE loss of activity has several deleterious effects on beta-cell function depending on when and how long it is inhibited and/or absent. In light of this, our results raise concerns about the utility of IDE inhibitors as a treatment for diabetes.

Authorship

ICC and GP contributed to conception and design of the work. CMFD, BM, JFLA, PC, MAdlF, CDL, AM, ICC, and GP make substantial contributions to acquisition, analysis, and interpretation of data. CMFD, ICC and GP participated in drafting the manuscript. MAL provided the floxed IDE mouse line. MAL, ICC and GP participated in revising the manuscript critically for important intellectual content. The guarantors for the content of the article are German Perdomo and Irene Cózar-Castellano.

Conflict of interest

There are no known conflicts of interest associated with this publication and there has been no significant financial support for this work that could have influenced its outcome. The manuscript has been read and approved by all named authors and that there are no other persons who satisfied the criteria for authorship but are not listed. The order of authors listed in the manuscript has been approved by all of us.

Funding

569 This work was supported by grants from the Spanish Ministry of Economy and Competitivity
570 (SAF2014-58702-C2-1-R and SAF2016-77871-C2-1-R to ICC; SAF2014-58702-C2-2-R and
571 SAF2016-77871-C2-2-R to GP), Fundacion La Caixa y Fundación Caja de Burgos (CAIXA-UBU001)
572 to GP, by grants from the American Diabetes Association (7-11-CD-14) and the National
573 Institutes of Health (GM115617) to MAL, and by a grant from Junta de Castilla y León, Spain
574 (VA114P17) to MAdlF.

575

576 **Acknowledgments**

577 Authors acknowledge Dr. Adolfo Garcia-Ocana (Mount Sinai School of Medicine, NY, USA) and
578 Dr. Maureen Gannon (University of Vanderbilt, TN, USA) for their thoughtful discussions of the
579 ideas in this report.

580

581

582 **References**

583 1. **Abdul-Hay SO, Kang D, McBride M, Li L, Zhao J, and Leissring MA**. Deletion of insulin-
584 degrading enzyme elicits antipodal, age-dependent effects on glucose and insulin tolerance.
585 *PLoS One* 6: e20818, 2011.
586 2. **Blum B, Hrvatin S, Schuetz C, Bonal C, Rezania A, and Melton DA**. Functional beta-cell
587 maturation is marked by an increased glucose threshold and by expression of urocortin 3. *Nat*
588 *Biotechnol* 30: 261-264, 2012.
589 3. **Coppieters KT, Wiberg A, Amirian N, Kay TW, and von Herrath MG**. Persistent glucose
590 transporter expression on pancreatic beta cells from longstanding type 1 diabetic individuals.
591 *Diabetes Metab Res Rev* 27: 746-754, 2011.
592 4. **Cotsapas C, Prokunina-Olsson L, Welch C, Saxena R, Weaver C, Usher N, Guiducci C,**
593 **Bonakdar S, Turner N, LaCroix B, and Hall JL**. Expression analysis of loci associated with type 2
594 diabetes in human tissues. *Diabetologia* 53: 2334-2339, 2010.
595 5. **Cozar-Castellano I, Takane KK, Bottino R, Balamurugan AN, and Stewart AF**. Induction
596 of beta-cell proliferation and retinoblastoma protein phosphorylation in rat and human islets
597 using adenovirus-mediated transfer of cyclin-dependent kinase-4 and cyclin D1. *Diabetes* 53:
598 149-159, 2004.
599 6. **Deprez-Poulain R, Hennuyer N, Bosc D, Liang WG, Enee E, Marechal X, Charton J,**
600 **Totobenazara J, Berte G, Jahklal J, Verdelet T, Dumont J, Dassonneville S, Woitrain E, Gauriot**
601 **M, Paquet C, Duplan I, Hermant P, Cantrelle FX, Sevin E, Culot M, Landry V, Herledan A,**
602 **Piveteau C, Lippens G, Leroux F, Tang WJ, van Endert P, Staels B, and Deprez B**. Catalytic site
603 inhibition of insulin-degrading enzyme by a small molecule induces glucose intolerance in mice.
604 *Nat Commun* 6: 8250, 2015.
605 7. **Duckworth WC**. Insulin degradation: mechanisms, products, and significance. *Endocr*
606 *Rev* 9: 319-345, 1988.
607 8. **Duckworth WC, Bennett RG, and Hamel FG**. Insulin degradation: progress and potential.
608 *Endocr Rev* 19: 608-624, 1998.
609 9. **Durham TB, Toth JL, Klimkowski VJ, Cao JX, Siesky AM, Alexander-Chacko J, Wu GY,**
610 **Dixon JT, McGee JE, Wang Y, Guo SY, Cavitt RN, Schindler J, Thibodeaux SJ, Calvert NA, Coghlan**
611 **MJ, Sindelar DK, Christe M, Kiselyov VV, Michael MD, and Sloop KW**. Dual Exosite-binding
612 Inhibitors of Insulin-degrading Enzyme Challenge Its Role as the Primary Mediator of Insulin
613 Clearance in Vivo. *J Biol Chem* 290: 20044-20059, 2015.
614 10. **Farris W, Mansourian S, Chang Y, Lindsley L, Eckman EA, Frosch MP, Eckman CB, Tanzi**
615 **RE, Selkoe DJ, and Guenette S**. Insulin-degrading enzyme regulates the levels of insulin, amyloid
616 beta-protein, and the beta-amyloid precursor protein intracellular domain in vivo. *Proc Natl*
617 *Acad Sci U S A* 100: 4162-4167, 2003.
618 11. **Fernandez-Diaz CM, Escobar-Curbelo L, Lopez-Acosta JF, Lobaton CD, Moreno A, Sanz-**
619 **Ortega J, Perdomo G, and Cozar-Castellano I**. Insulin degrading enzyme is up-regulated in
620 pancreatic beta cells by insulin treatment. *Histol Histopathol* 33: 1167-1180, 2018.
621 12. **Furukawa Y, Shimada T, Furuta H, Matsuno S, Kusuyama A, Doi A, Nishi M, Sasaki H,**
622 **Sanke T, and Nanjo K**. Polymorphisms in the IDE-KIF11-HHEX gene locus are reproducibly
623 associated with type 2 diabetes in a Japanese population. *J Clin Endocrinol Metab* 93: 310-314,
624 2008.
625 13. **Furuta M, Carroll R, Martin S, Swift HH, Ravazzola M, Orci L, and Steiner DF**. Incomplete
626 processing of proinsulin to insulin accompanied by elevation of Des-31,32 proinsulin
627 intermediates in islets of mice lacking active PC2. *J Biol Chem* 273: 3431-3437, 1998.
628 14. **Henquin J-C, and Nenquin M**. Immaturity of insulin secretion by pancreatic islets
629 isolated from one human neonate. *Journal of diabetes investigation* 9: 270-273, 2018.
630 15. **Herrera PL, Orci L, and Vassalli JD**. Two transgenic approaches to define the cell lineages
631 in endocrine pancreas development. *Mol Cell Endocrinol* 140: 45-50, 1998.

16. **Hou JC, Min L, and Pessin JE**. Insulin granule biogenesis, trafficking and exocytosis. *Vitam Horm* 80: 473-506, 2009.
17. **Hu C, Zhang R, Wang C, Wang J, Ma X, Lu J, Qin W, Hou X, Wang C, Bao Y, Xiang K, and Jia W**. PPARG, KCNJ11, CDKAL1, CDKN2A-CDKN2B, IDE-KIF11-HHEX, IGF2BP2 and SLC30A8 are associated with type 2 diabetes in a Chinese population. *PLoS One* 4: e7643, 2009.
18. **Huang C, Walker EM, Dadi PK, Hu R, Xu Y, Zhang W, Sanavia T, Mun J, Liu J, Nair GG, Tan HYA, Wang S, Magnuson MA, Stoeckert CJ, Jr., Hebrok M, Gannon M, Han W, Stein R, Jacobson DA, and Gu G**. Synaptotagmin 4 Regulates Pancreatic beta Cell Maturation by Modulating the Ca(2+) Sensitivity of Insulin Secretion Vesicles. *Dev Cell* 45: 347-361 e345, 2018.
19. **Hyslop CM, Tsai S, Shrivastava V, Santamaria P, and Huang C**. Prolactin as an Adjunct for Type 1 Diabetes Immunotherapy. *Endocrinology* 157: 150-165, 2016.
20. **Jimenez-Palomares M, Ramos-Rodriguez JJ, Lopez-Acosta JF, Pacheco-Herrero M, Lechuga-Sancho AM, Perdomo G, Garcia-Alloza M, and Cozar-Castellano I**. Increased Abeta production prompts the onset of glucose intolerance and insulin resistance. *Am J Physiol Endocrinol Metab* 302: E1373-1380, 2012.
21. **Kanety H, Moshe S, Shafrir E, Lunenfeld B, and Karasik A**. Hyperinsulinemia induces a reversible impairment in insulin receptor function leading to diabetes in the sand rat model of non-insulin-dependent diabetes mellitus. *Proc Natl Acad Sci U S A* 91: 1853-1857, 1994.
22. **Kropp PA, Dunn JC, Carboneau BA, Stoffers DA, and Gannon M**. Cooperative function of Pdx1 and Oc1 in multipotent pancreatic progenitors impacts postnatal islet maturation and adaptability. *Am J Physiol Endocrinol Metab* 314: E308-E321, 2018.
23. **Lachaal M, Spangler RA, and Jung CY**. High Km of GLUT-2 glucose transporter does not explain its role in insulin secretion. *Am J Physiol* 265: E914-919, 1993.
24. **Leissring MA, Malito E, Hedouin S, Reinstatler L, Sahara T, Abdul-Hay SO, Choudhry S, Maharvi GM, Fauq AH, Huzarska M, May PS, Choi S, Logan TP, Turk BE, Cantley LC, Manolopoulou M, Tang WJ, Stein RL, Cuny GD, and Selkoe DJ**. Designed inhibitors of insulin-degrading enzyme regulate the catabolism and activity of insulin. *PLoS One* 5: e10504, 2010.
25. **Maeda Y, Akazawa S, Akazawa M, Takao Y, Trocino RA, Takino H, Kawasaki E, Yokota A, Okuno S, and Nagataki S**. Glucose transporter gene expression in rat conceptus during early organogenesis and exposure to insulin-induced hypoglycemic serum. *Acta Diabetol* 30: 73-78, 1993.
26. **Maianti JP, McFedries A, Foda ZH, Kleiner RE, Du XQ, Leissring MA, Tang WJ, Charron MJ, Seeliger MA, Saghatelian A, and Liu DR**. Anti-diabetic activity of insulin-degrading enzyme inhibitors mediated by multiple hormones. *Nature* 511: 94-98, 2014.
27. **Mirsky IA, and Broh-Kahn RH**. The inactivation of insulin by tissue extracts; the distribution and properties of insulin inactivating extracts. *Arch Biochem* 20: 1-9, 1949.
28. **Najjar SM, and Perdomo G**. Hepatic Insulin Clearance: Mechanism and Physiology. *Physiology* 34: 198-215, 2019.
29. **Pascoe L, Tura A, Patel SK, Ibrahim IM, Ferrannini E, Zeggini E, Weedon MN, Mari A, Hattersley AT, McCarthy MI, Frayling TM, Walker M, Consortium R, and Consortium UKTDG**. Common variants of the novel type 2 diabetes genes CDKAL1 and HHEX/IDE are associated with decreased pancreatic beta-cell function. *Diabetes* 56: 3101-3104, 2007.
30. **Pivovarova O, Hohn A, Grune T, Pfeiffer AF, and Rudovich N**. Insulin-degrading enzyme: new therapeutic target for diabetes and Alzheimer's disease? *Ann Med* 48: 614-624, 2016.
31. **Puri S, Roy N, Russ HA, Leonhardt L, French EK, Roy R, Bengtsson H, Scott DK, Stewart AF, and Hebrok M**. Replication confers β cell immaturity. *Nature Communications* 9: 485, 2018.
32. **Shanik MH, Xu Y, Skrha J, Dankner R, Zick Y, and Roth J**. Insulin resistance and hyperinsulinemia: is hyperinsulinemia the cart or the horse? *Diabetes Care* 31 Suppl 2: S262-268, 2008.
33. **Sladek R, Rocheleau G, Rung J, Dina C, Shen L, Serre D, Boutin P, Vincent D, Belisle A, Hadjadj S, Balkau B, Heude B, Charpentier G, Hudson TJ, Montpetit A, Pshezhetsky AV, Prentki**

M, Posner BI, Balding DJ, Meyre D, Polychronakos C, and Froguel P. A genome-wide association study identifies novel risk loci for type 2 diabetes. *Nature* 445: 881-885, 2007.
34. **Steneberg P, Bernardo L, Edfalk S, Lundberg L, Backlund F, Ostenson CG, and Edlund H**. The type 2 diabetes-associated gene ide is required for insulin secretion and suppression of alpha-synuclein levels in beta-cells. *Diabetes* 62: 2004-2014, 2013.
35. **Tal M, Thorens B, Surana M, Fleischer N, F Lodish H, Hanahan D, and Efrat S**. *Glucose transporter isotypes switch in T-antigen-transformed pancreatic β cells growing in culture and in mice*. 1992, p. 422-432.
36. **Talchai C, Xuan S, Lin HV, Sussel L, and Accili D**. Pancreatic beta cell dedifferentiation as a mechanism of diabetic beta cell failure. *Cell* 150: 1223-1234, 2012.
37. **Templeman NM, Flibotte S, Chik JHL, Sinha S, Lim GE, Foster LJ, Nislow C, and Johnson JD**. Reduced Circulating Insulin Enhances Insulin Sensitivity in Old Mice and Extends Lifespan. *Cell reports* 20: 451-463, 2017.
38. **Thorens B**. GLUT2, glucose sensing and glucose homeostasis. *Diabetologia* 58: 221-232, 2015.
39. **van der Meulen T, Mawla AM, DiGruccio MR, Adams MW, Nies V, Dolleman S, Liu S, Ackermann AM, Caceres E, Hunter AE, Kaestner KH, Donaldson CJ, and Huising MO**. Virgin Beta Cells Persist throughout Life at a Neogenic Niche within Pancreatic Islets. *Cell Metab* 25: 911-926 e916, 2017.
40. **Villa-Perez P, Merino B, Fernandez-Diaz CM, Cidad P, Lobaton CD, Moreno A, Muturi HT, Ghadieh HE, Najjar SM, Leissring MA, Cozar-Castellano I, and Perdomo G**. Liver-specific ablation of insulin-degrading enzyme causes hepatic insulin resistance and glucose intolerance, without affecting insulin clearance in mice. *Metabolism* 88: 1-11, 2018.
41. **Wicksteed B, Brissova M, Yan W, Opland DM, Plank JL, Reinert RB, Dickson LM, Tamarina NA, Philipson LH, Shostak A, Bernal-Mizrachi E, Elghazi L, Roe MW, Labosky PA, Myers MG, Jr., Gannon M, Powers AC, and Dempsey PJ**. Conditional gene targeting in mouse pancreatic ss-Cells: analysis of ectopic Cre transgene expression in the brain. *Diabetes* 59: 3090-3098, 2010.
42. **Wu Y, Li H, Loos RJ, Yu Z, Ye X, Chen L, Pan A, Hu FB, and Lin X**. Common variants in CDKAL1, CDKN2A/B, IGF2BP2, SLC30A8, and HHEX/IDE genes are associated with type 2 diabetes and impaired fasting glucose in a Chinese Han population. *Diabetes* 57: 2834-2842, 2008.
43. **Zhu X, Zhou A, Dey A, Norrbom C, Carroll R, Zhang C, Laurent V, Lindberg I, Ugleholdt R, Holst JJ, and Steiner DF**. Disruption of PC1/3 expression in mice causes dwarfism and multiple neuroendocrine peptide processing defects. *Proc Natl Acad Sci U S A* 99: 10293-10298, 2002.

Figure Legends

Figure 1: Impaired insulin secretion after transient IDE inhibition in vitro in beta-cells. (A) Representative IDE western blot of INS-1E cells untreated, transfected with siRNA-Control or siRNA-IDE. (B) Quantification of IDE by western blotting in INS-1E cells. n= 4 independent experiments in triplicates. (C) GSIS (glucose-stimulated insulin secretion) in siRNA-transfected INS-1E cells exposed to low or high glucose concentrations. n= 3 independent experiments in triplicates. (D) C-peptide levels after GSIS in INS-1E cells. n= 3 different experiments in triplicates. (E) Intracellular insulin content of siRNA-transfected INS-1E cells. n= 3 independent experiments in triplicates. Data are presented as mean ± SEM. *p< 0.05 versus siRNA-C condition; §p< 0.05 versus low glucose by two-way ANOVA.

Figure 2: Impaired insulin secretion after chronic IDE inhibition in vitro in beta-cells. (A) Representative IDE western blot of INS-1E cells transfected with shRNA-Control or shRNA-IDE. (B) Quantification of IDE by western blotting in INS-1E cells. n= 3 independent experiments in duplicates. (C) GSIS (glucose-stimulated insulin secretion) in INS-1E cells exposed to low or high glucose concentrations. n= 3 independent experiments in triplicates. (D) Intracellular insulin content of shRNA INS-1E cells. n= 3 independent experiments in triplicates. (E) Quantification of insulin vesicle density in shRNA-Control or shRNA-IDE INS1 cells after GSIS. n=16-21 cells per condition. (F) Representative images acquired by electron microscopy from shRNA INS-1E cells. Data are presented as mean ± SEM. *p< 0.05 versus Ctrl condition; §p< 0.05 versus low glucose by two-way ANOVA. Data are presented as mean ± SEM. *p< 0.05 versus shRNA-C condition; §p< 0.05 versus low glucose by two-way ANOVA.

Figure 3: Impaired insulin secretion after pharmacological IDE inhibition in vitro in pancreatic rat and human islets. (A) Insulin secretion from rat islets exposed to low or high glucose concentrations after 1h treatment with NTE-2. n=3 independent experiments in quintuplicates. (B) Insulin secretion from human islets exposed to low or high glucose concentrations after 1h treatment with NTE-2. n= 2 in triplicates (from two independent human islet preparations). Data are presented as mean ± SEM. *p< 0.05 versus vehicle/control condition; §p< 0.05 versus low glucose by two-way ANOVA.

Figure 4: IDE loss of expression in pancreatic beta-cells of B-IDE-KO mice. (A) Breeding strategy to obtain B-IDE-KO mice. (B) IDE expression in different tissues measured by quantitative PCR. n=3 WT; n=2 B-IDE-KO in duplicate. (C) Representative IDE western blot in islets of WT (*Ide$^{flox/flox}$; +/+* or *Ide$^{flox/+}$; +/+*), B-IDE-HT (*Ide$^{flox/+}$; Ins-Cre/+*), B-IDE-KO (*Ide$^{flox/flox}$; Ins-Cre/+*) and T-IDE-KO (germ-line, Total-IDE-KO) mice. (D) IDE and insulin double-staining in WT and B-IDE- KO pancreata.

Figure 5: Characterization of B-IDE-KO mouse glucose homeostasis at 2 months of age. (A) Blood glucose levels after 16h fasting. (B) Blood glucose levels after 6h fasting. (C) Blood glucose levels in non-fasting. (D) IPGTT after 6h fasting. (E) Area under the curve of figure D. (F) Weight of animals (n=7 WT; n=7 B-IDE-KO). (G) Plasma C-peptide levels at 0, 5, 15 and 30 min after intraperitoneal injection of glucose (2 g/kg) (n=5 WT; n=7 B-IDE-KO). (H) Area under the curve of figure G. (I) GSIS (glucose-stimulated insulin secretion) in WT and B-IDE-KO islets exposed to low or high glucose concentrations. (n=9 WT; n=9 B-IDE-KO). (J) Fold-change of GSIS of figure E. *p< 0.05 versus WT condition; §p< 0.05 versus low glucose by two-way ANOVA.

Figure 6: Characterization of B-IDE-KO mouse glucose homeostasis at 6 months of age. (A) Blood glucose levels after 16h fasting. (B) Blood glucose levels after 6h fasting. (C) Blood glucose levels in non-fasting conditions. (n=13 WT; n=12 B-IDE-KO) (D) Plasma C-peptide levels after 6h fasting. (E) Plasma C-peptide levels in non-fasting conditions. (n=8 WT; n=5 B-IDE-KO) (F) IPGTT after 6h fasting. (G) Area under the curve of figure G. (H) Weight of animals. (n=13 WT; n=12 B-IDE-KO). (I) Hepatic gluconeogenic enzymes *Pck1* and *G6pc* were studied by RT-PCR to detect expression levels (n=5 WT; n=4 B-IDE-KO in triplicates). Data are presented as mean ± SEM*p < 0.05 by two-tailed Student's t test.

Figure 7: Increased plasma C-peptide levels are not due to increased B-IDE-KO beta-cell area but to constitute insulin secretion. (A) Plasma C-peptide levels at 0, 5, 15 and 30 min after intraperitoneal injection of glucose (2 g/kg) (n=7 WT; n=5 B-IDE-KO). (B) Area under the curve of figure A. (C) Quantification of beta-cell area per pancreas. (D) Representative images of insulin staining in pancreas from WT and B-IDE-KO mice. (E) Quantification of alpha-cell area. (F) Representative images of glucagon staining in pancreas from WT and B-IDE-KO mice. (G) Quantification of number of islets/pancreas area in WT and B-IDE-KO mice. (n=7 WT; n=10 B-IDE-KO for pancreas histomorphometry) (H) GSIS (glucose-stimulated insulin secretion) in WT and B-IDE-KO islets exposed to low or high glucose concentrations. (I) Fold-change of GSIS of figure E. (J) Intracellular insulin content of WT and B-IDE-KO islets. (K) Proinsulin release in WT and B-IDE-KO islets exposed to low or high glucose concentrations. (n=9 WT; n=12 B-IDE-KO). Data are presented as mean ± SEM. *p< 0.05 versus WT condition; §p< 0.05 versus low glucose by two-way ANOVA.

Figure 8: Disturbances in transcription factors and insulin secretory machinery proteins point to B-IDE-KO beta-cell functional immaturity. (A) Results of quantitative PCR experiments showing expression of different genes involved in beta-cell maturity; (B) beta-cell secretory machinery; and (C) insulin processing (protein convertase 1) normalized to L18 expression as housekeeping

gene in B-IDE-KO mice islets. Each column is the mean of islets from 3-6 different mice per group in duplicate for each condition. Data are expressed using the (2−ΔΔCt) formula ± SEM. *p < 0.05 determined by 2-tailed Student's t test.

Figure 9: Glucose transporters show an abnormal pattern in B-IDE-KO beta-cells. (A) Representative images of Glut2 immunofluorescence in pancreas of WT and B-IDE-KO mice (n=6 WT; n=7 B-IDE-KO). (B) Representative images of Glut1 immunofluorescence in pancreas of WT and B-IDE-KO mice (n=6 WT; n=6 B-IDE-KO). (C) Quantification of Glut1 staining intensity in pancreatic beta-cells. (D) Representative western-blot of IDE, GK, Glut1 and Glut2 protein expression in isolated islets of WT and B-IDE-KO mice. (E) Quantification of Glut1 WB. (F) Quantification of Glut2 WB. (G) Quantification of GK WB. (n=9 WT; n=6 B-IDE-KO) *p < 0.05 determined by 2-tailed Student's t test.

Supplementary Figures are available at: **https://doi.org/10.6084/m9.figshare.9675437.v1**

Figure 1

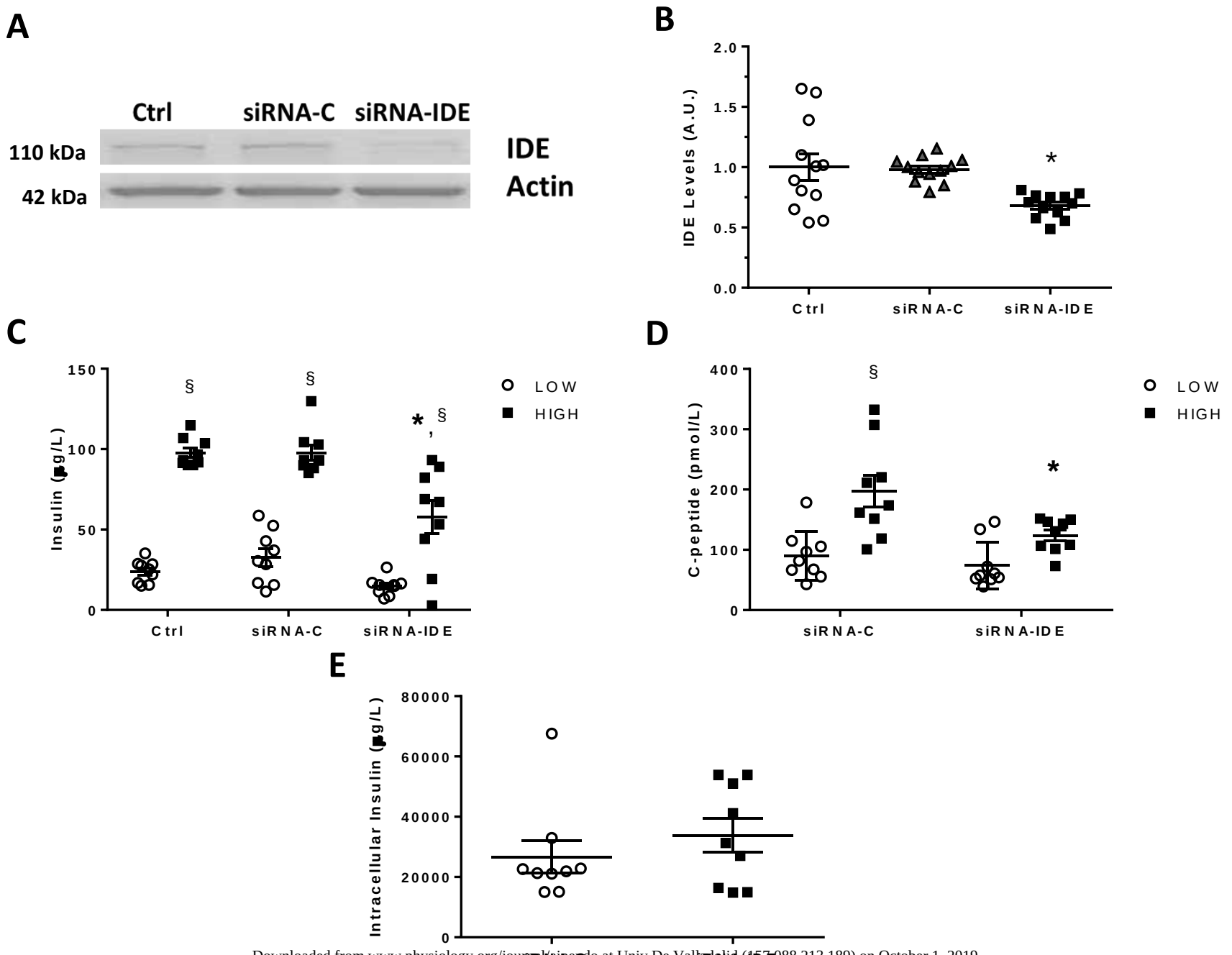

Figure 2

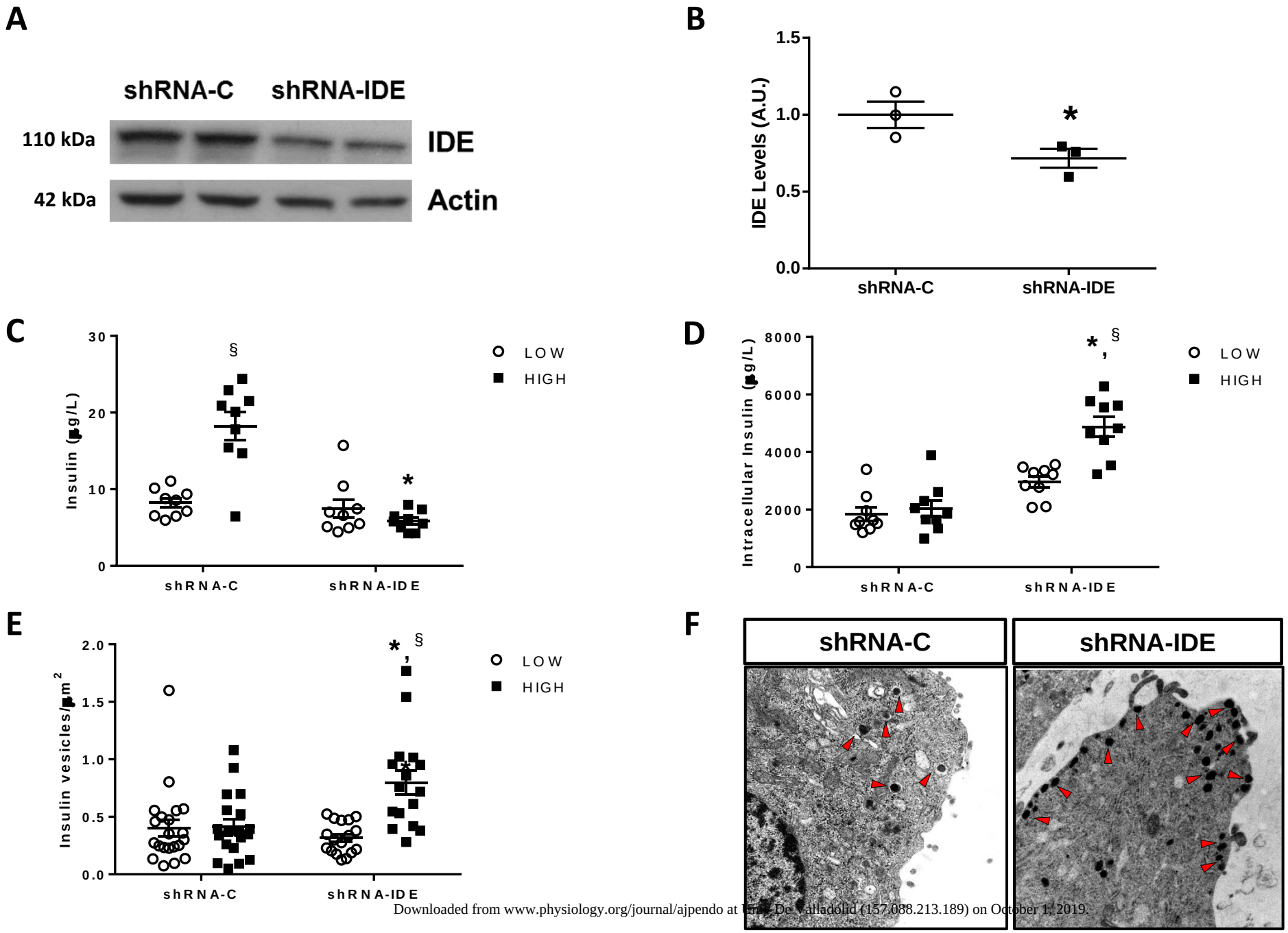

Figure 3

A

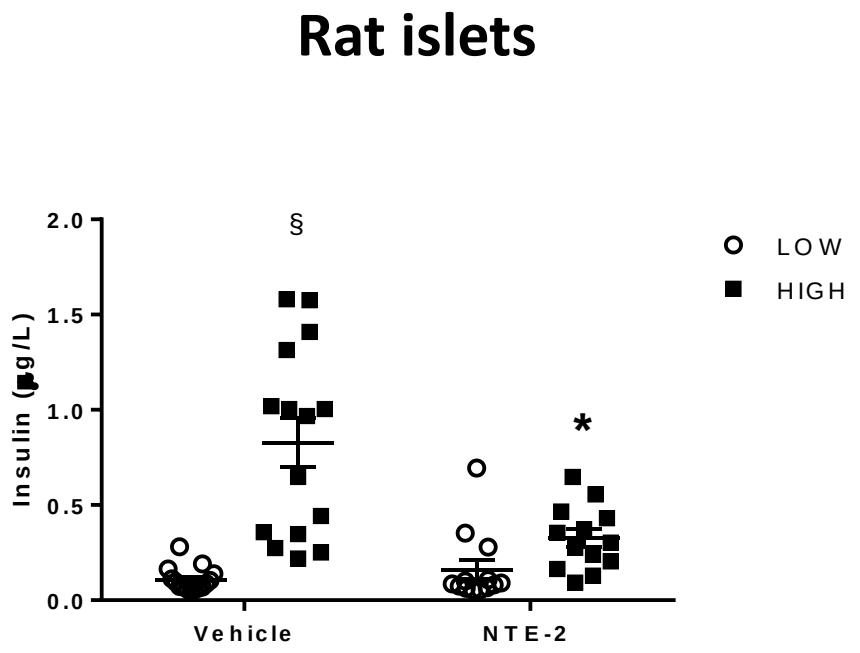

B

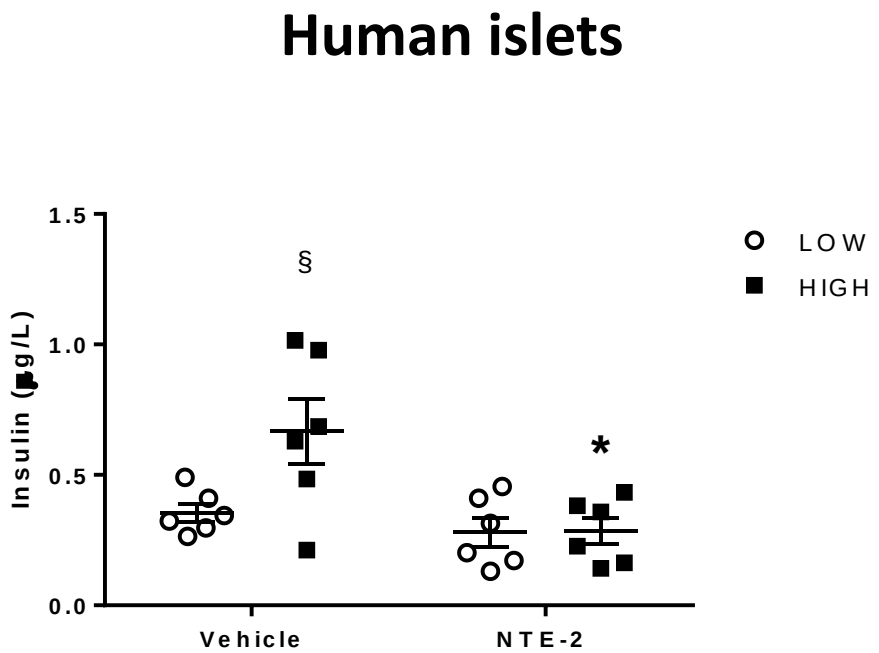

Figure 4

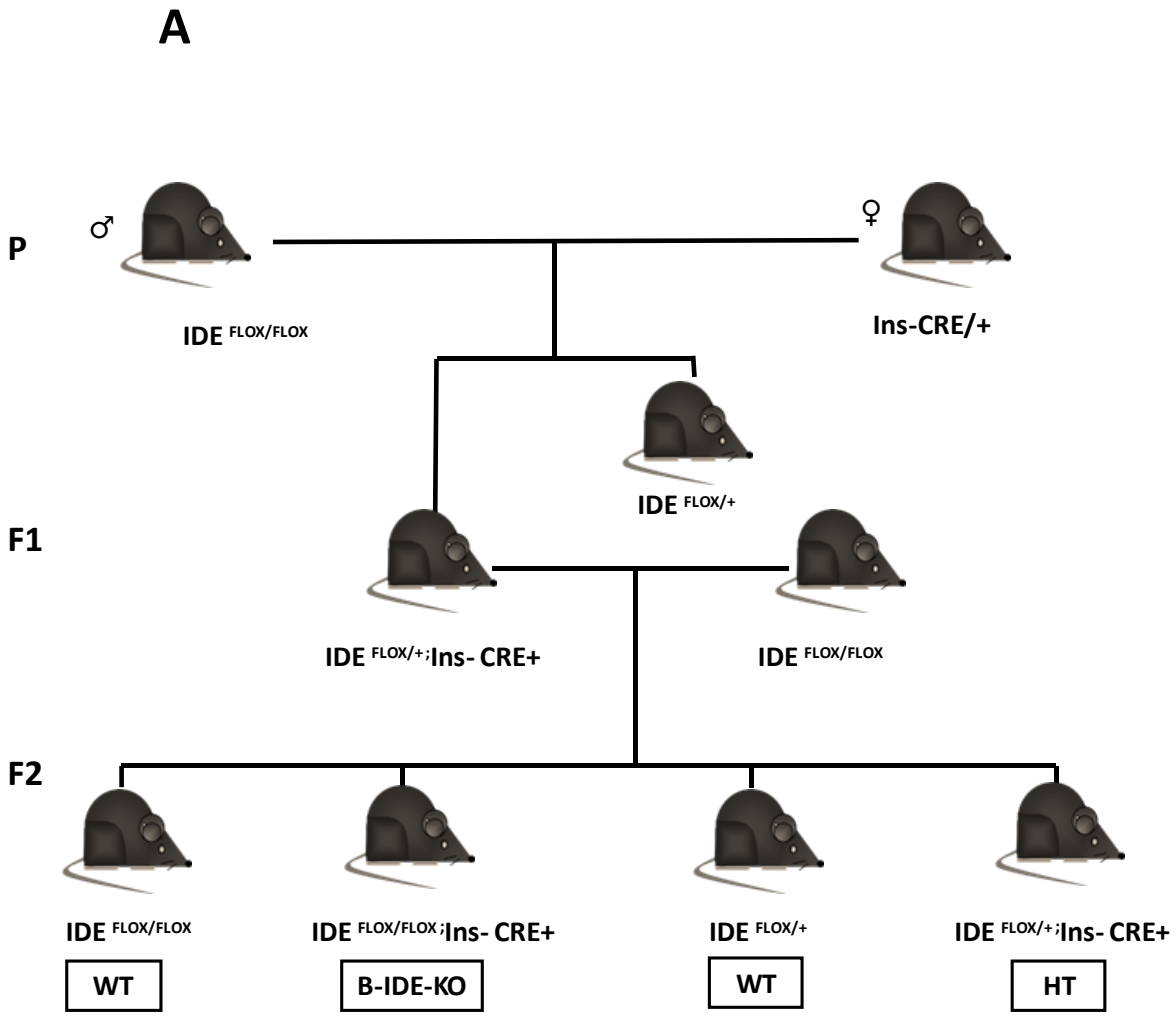

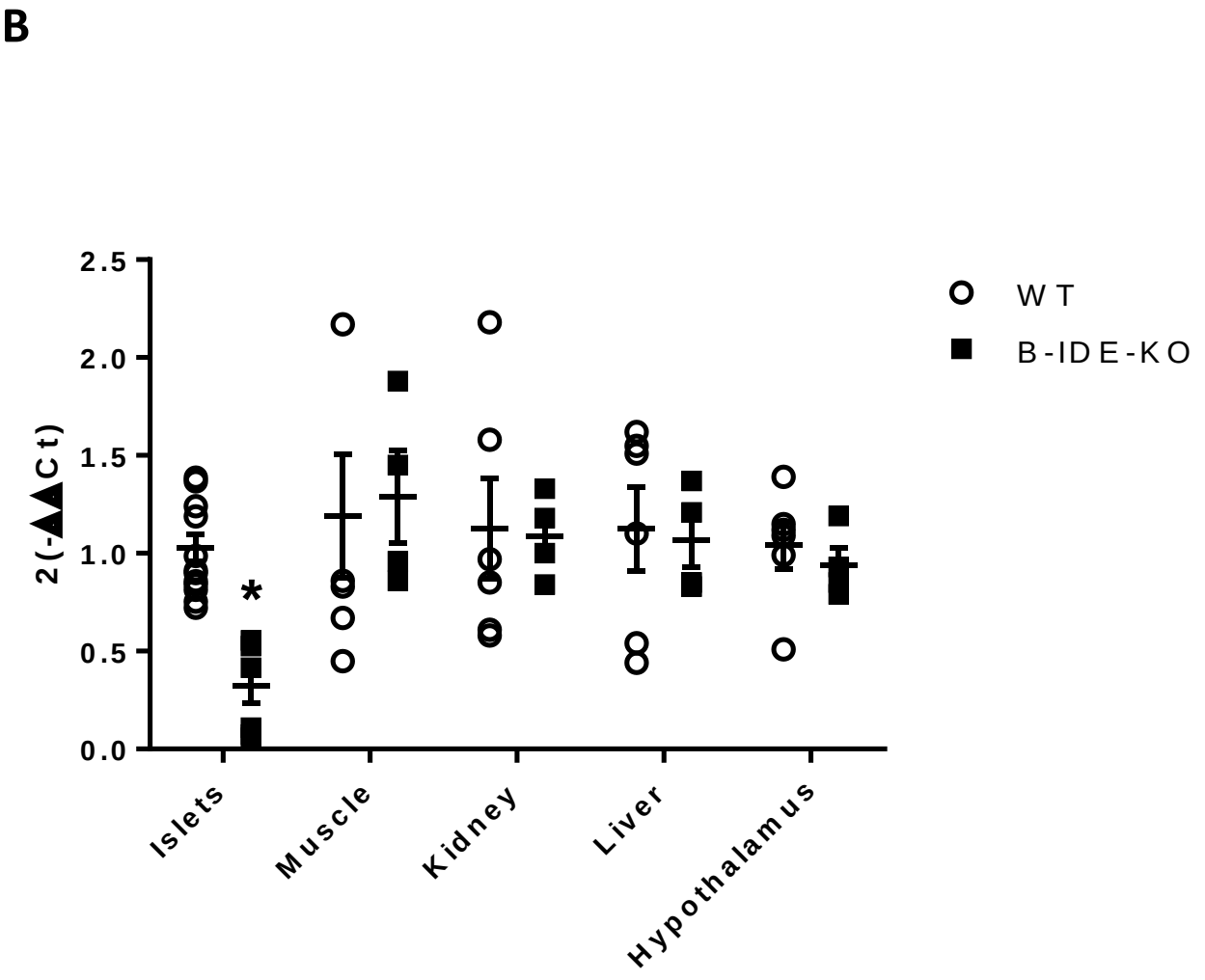

C

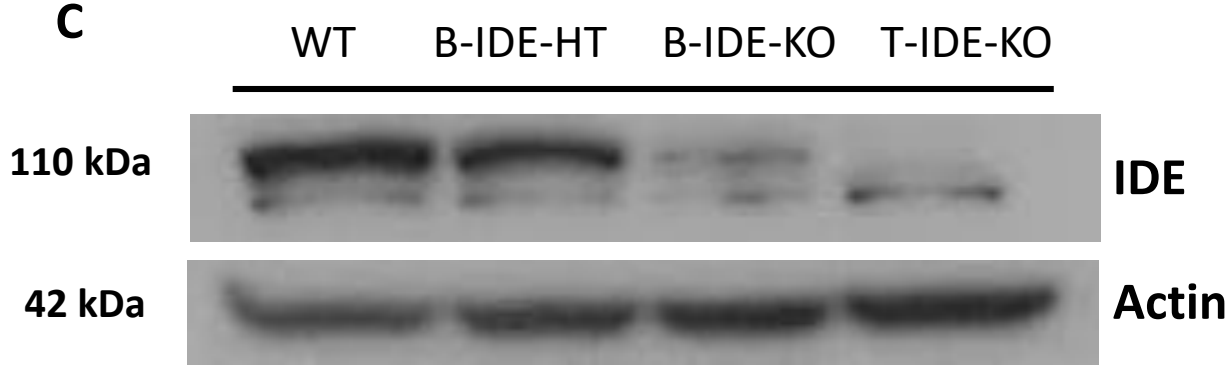

D

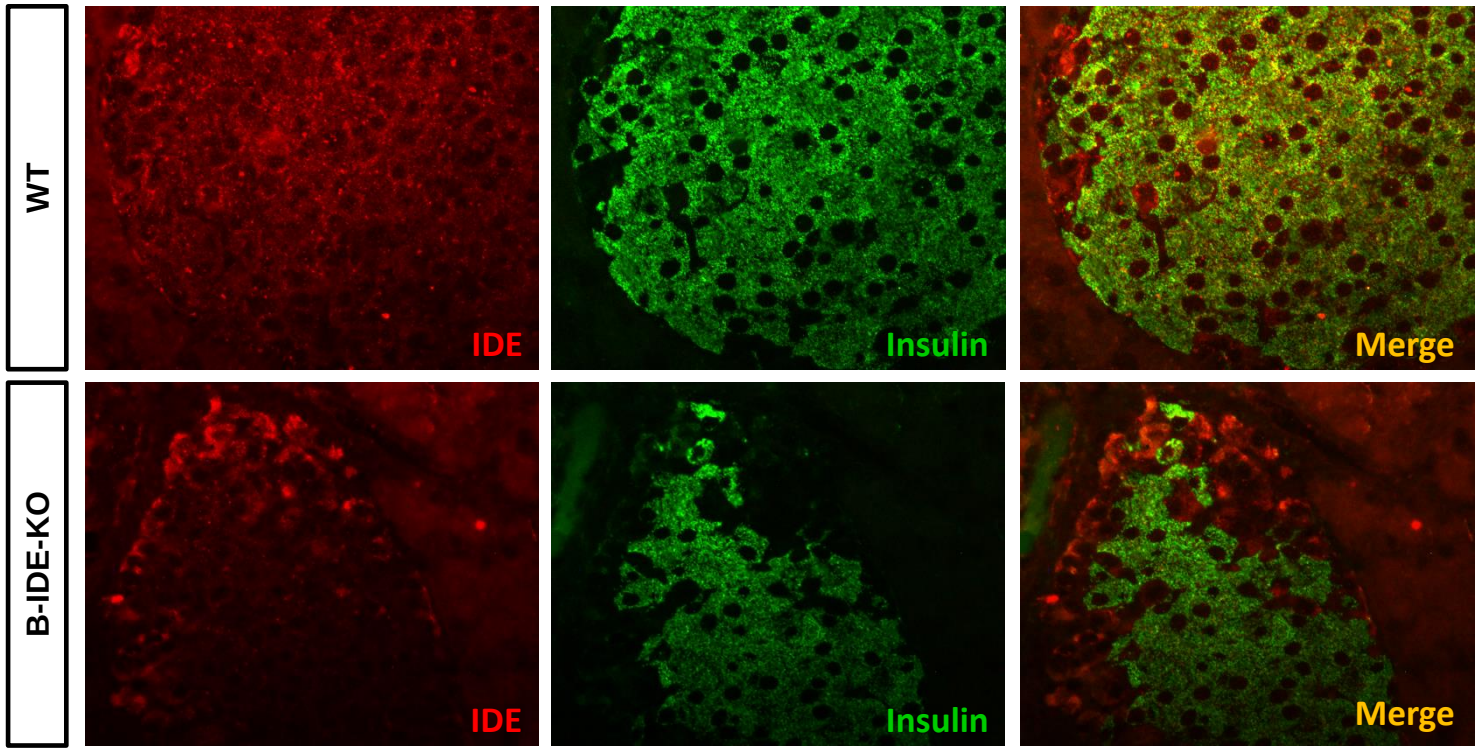

Figure 5

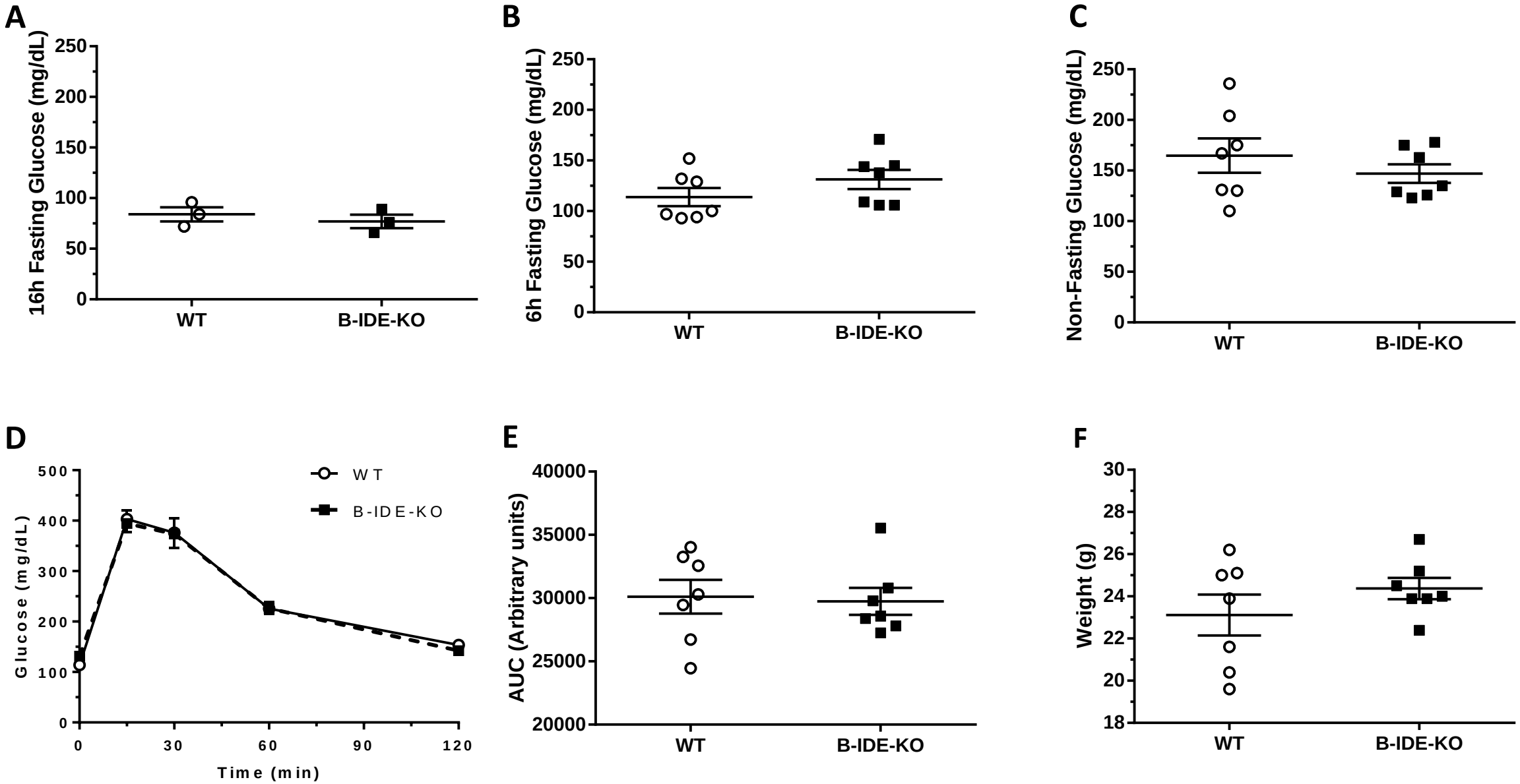

Figure 5

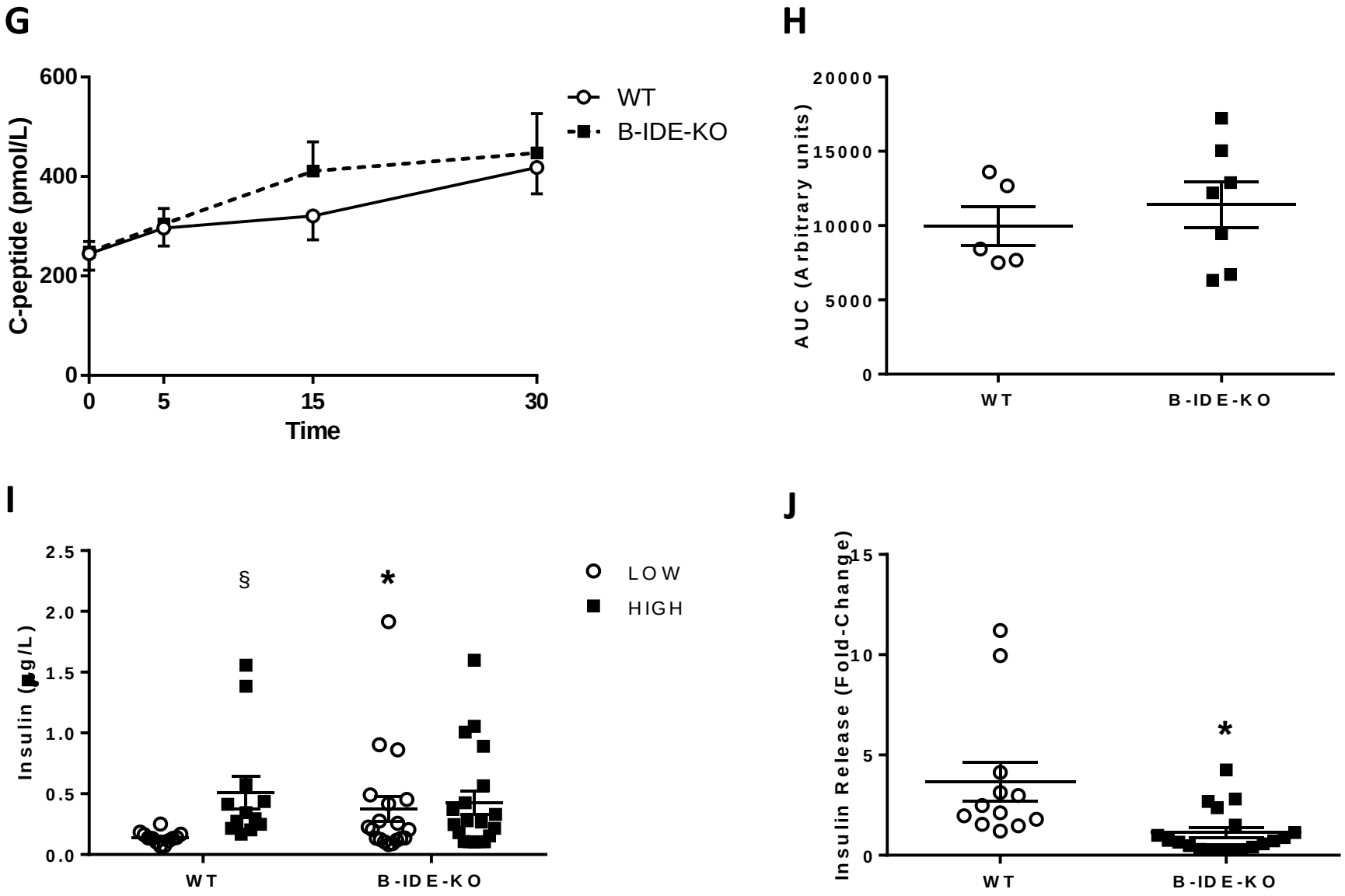

Figure 6

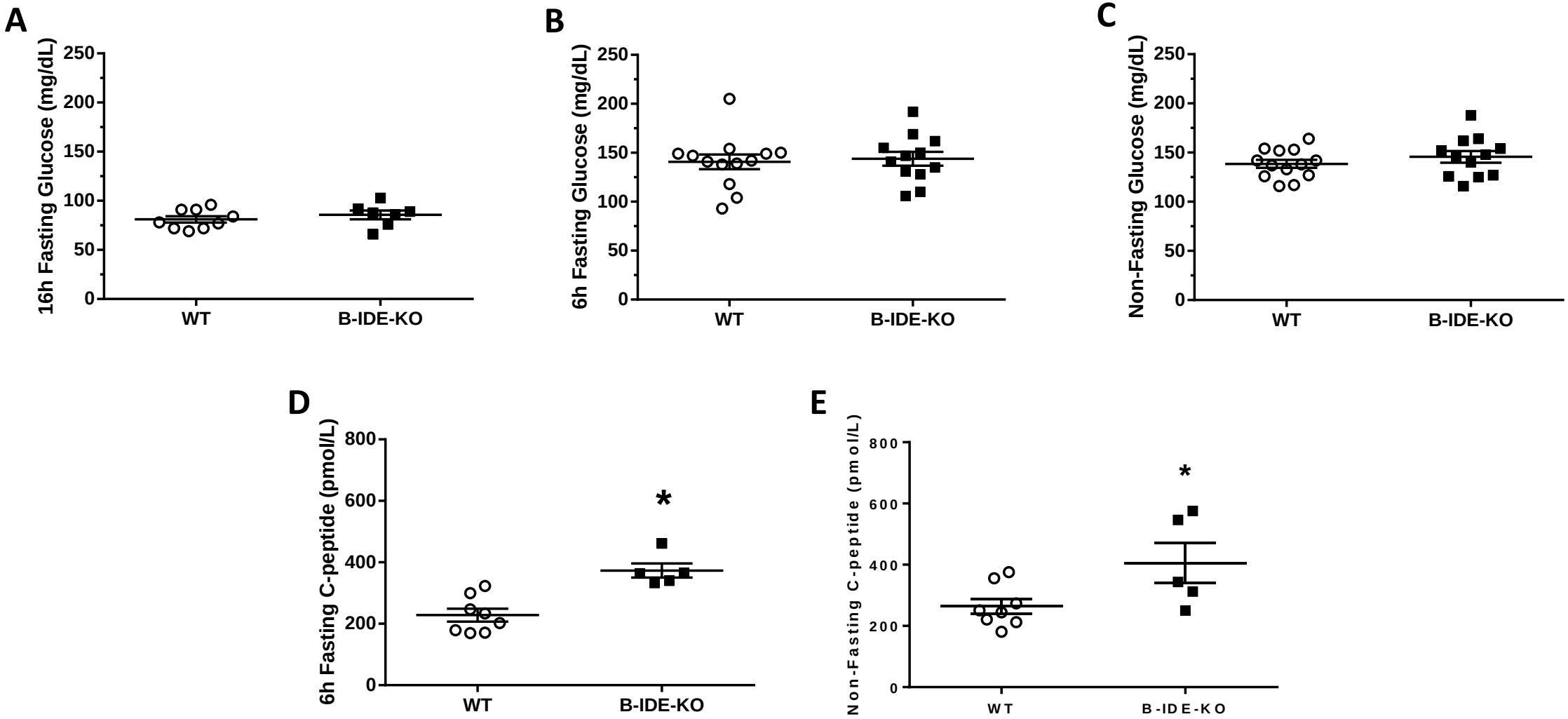

Figure 6

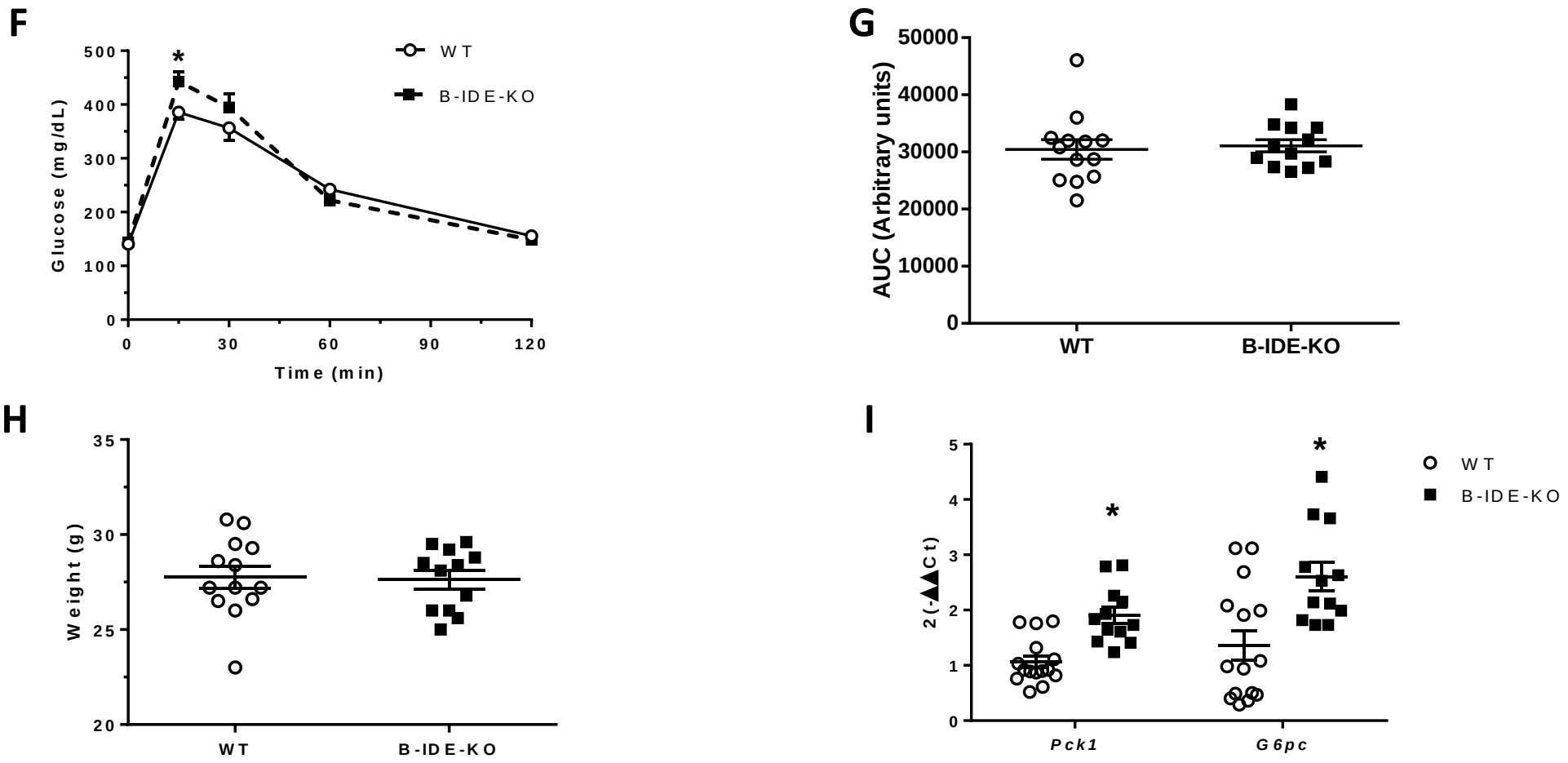

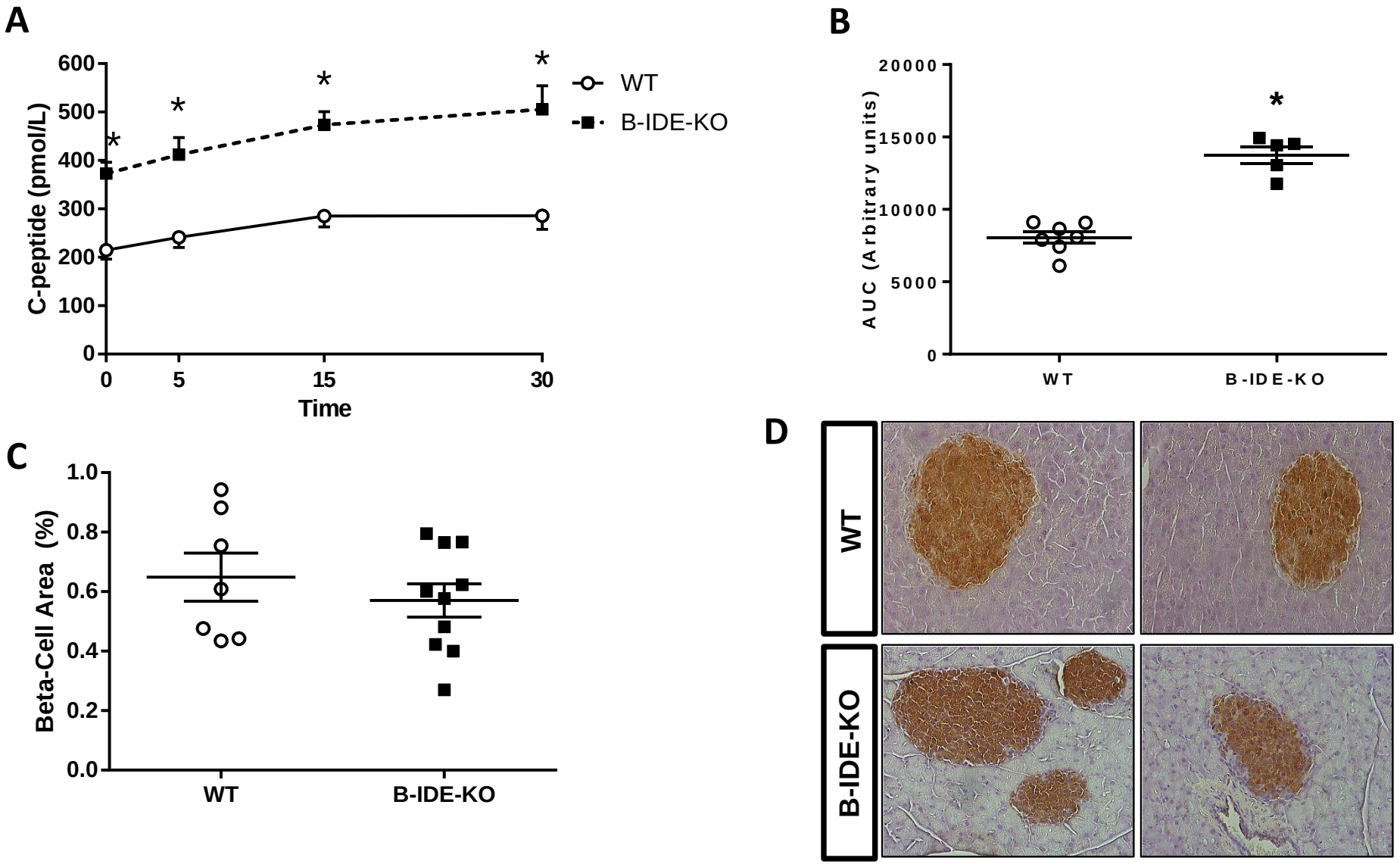

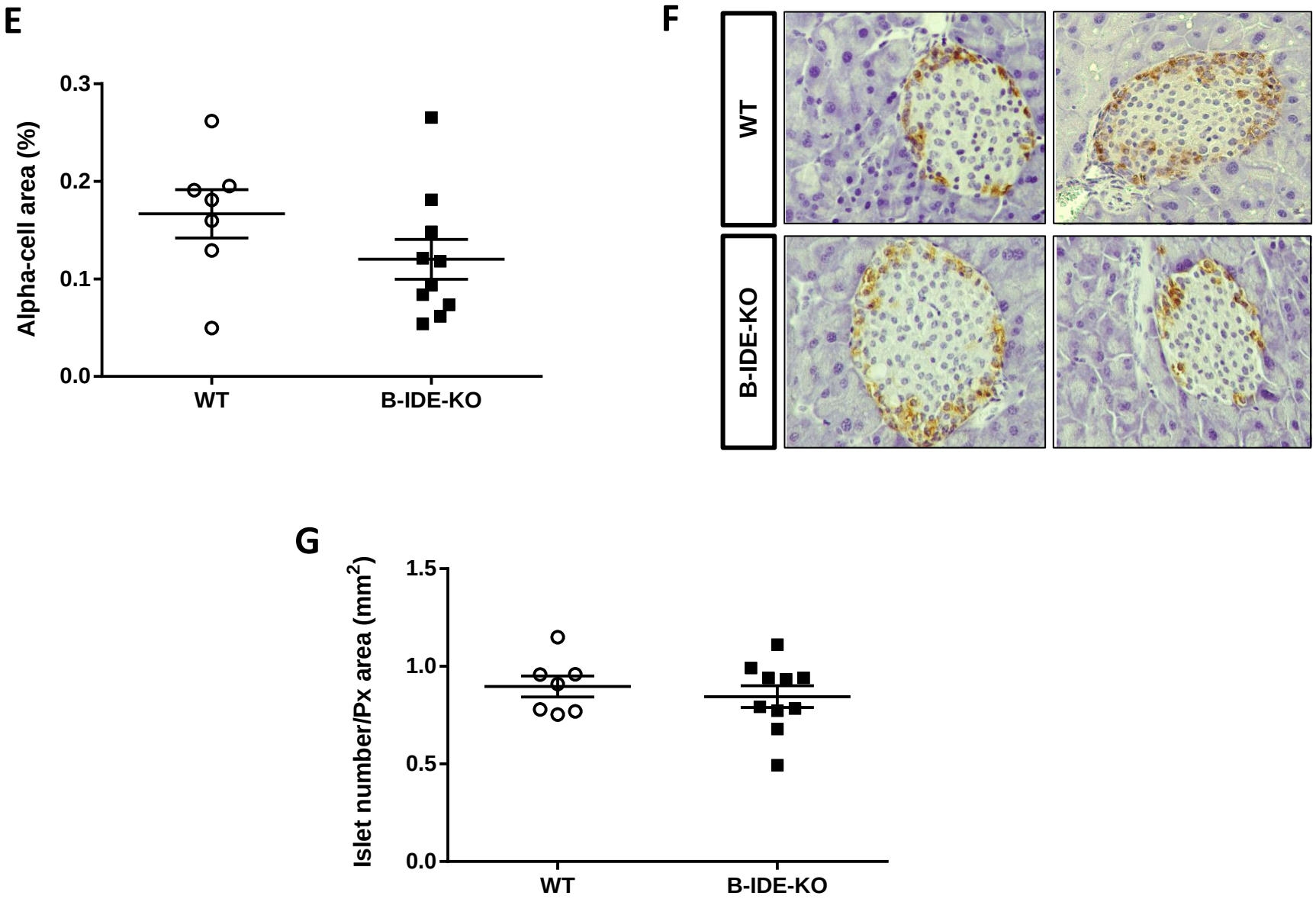

Figure 7

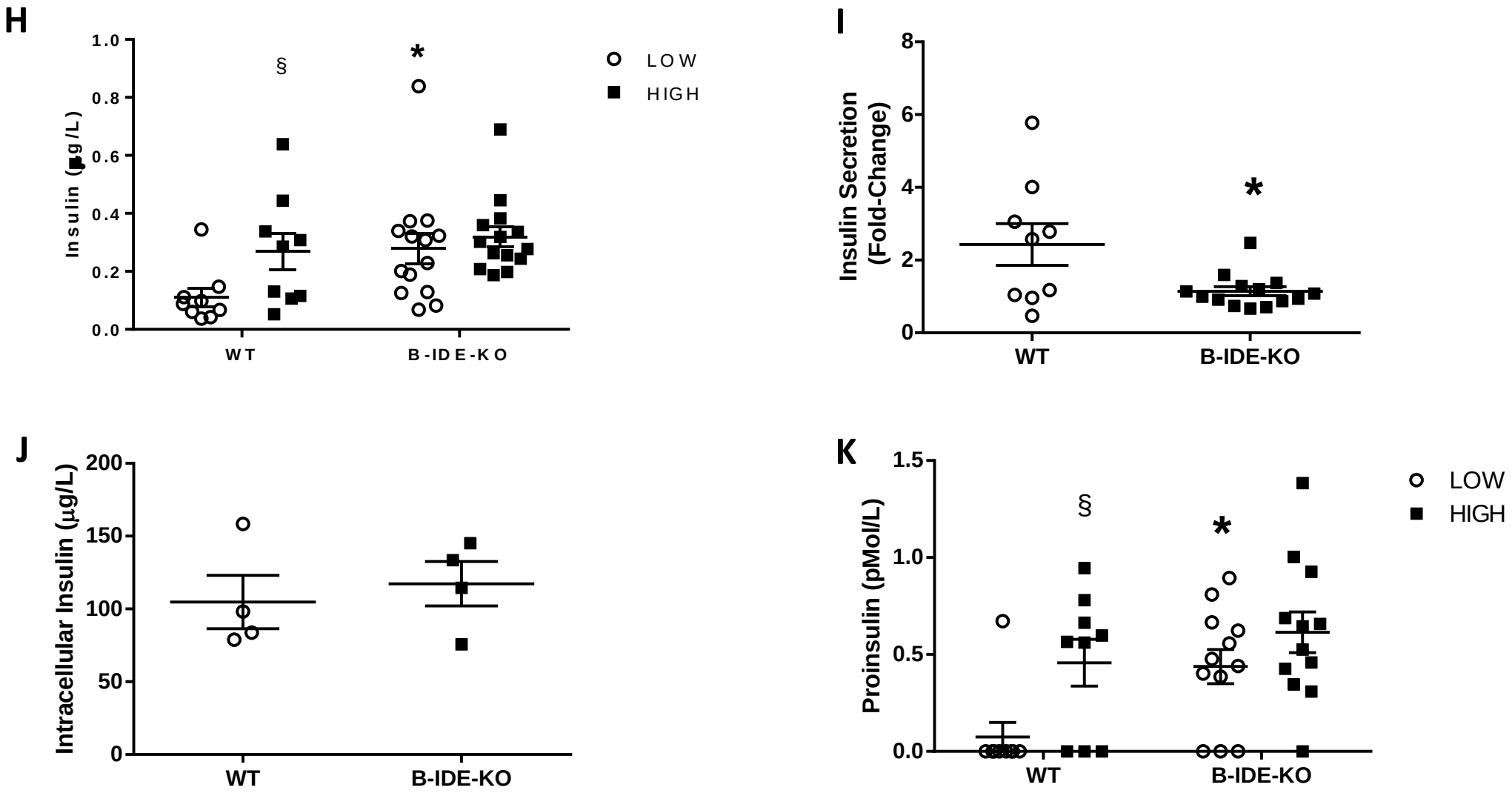

Figure 8

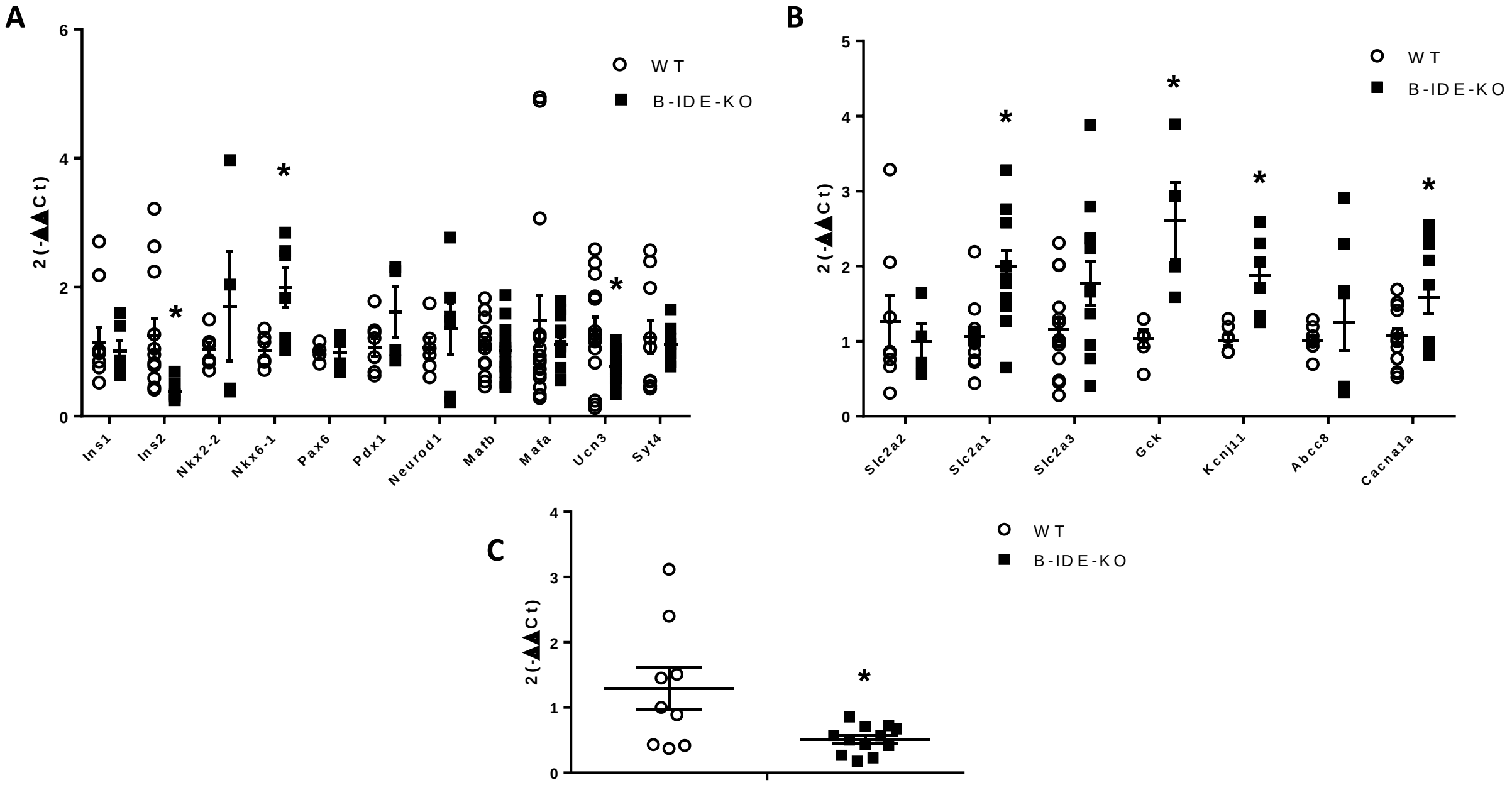

Figure 9

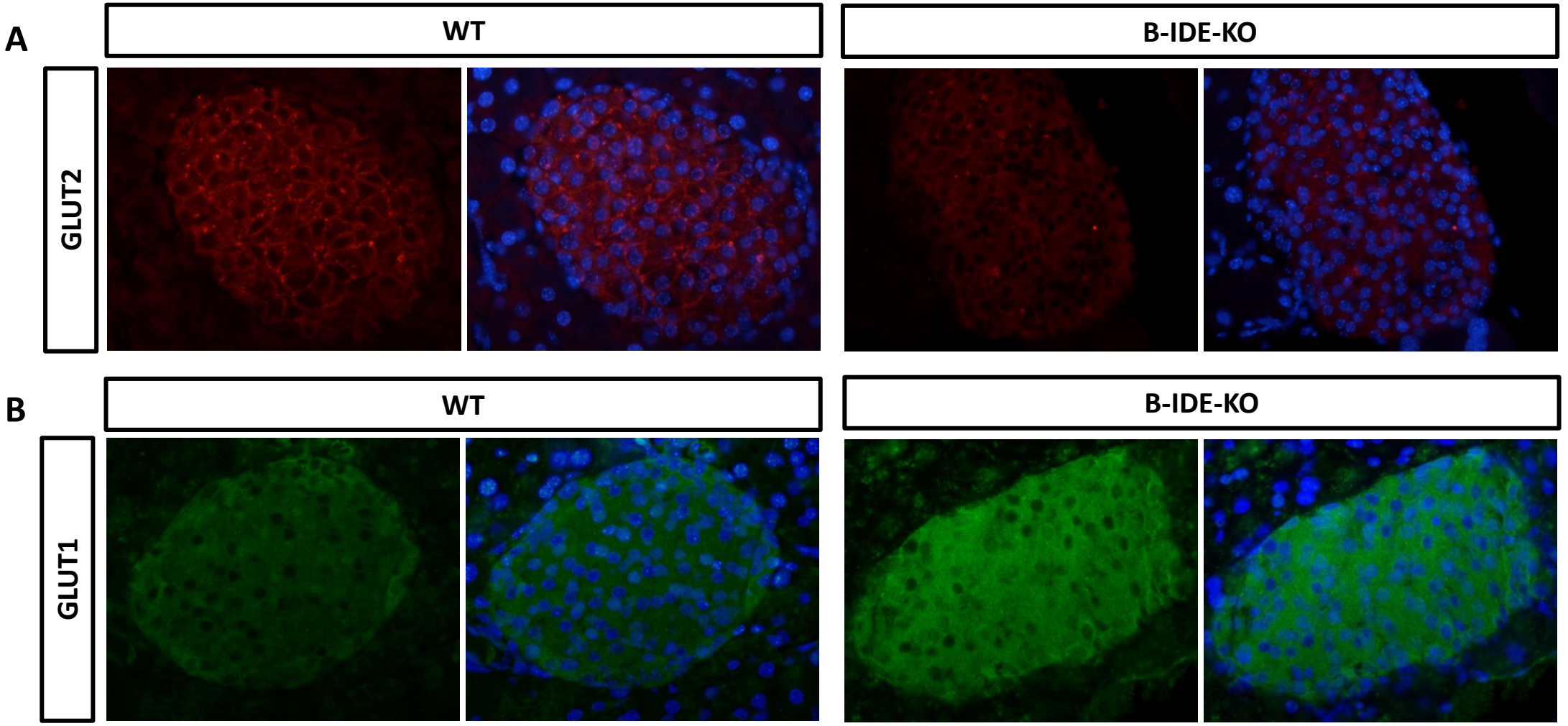

Figure 9